Self-Assembled Nanofiltration Membranes with Thermo- and pH-Responsive Behavior

Saadat, Younes
Kim, Kyungtae
Foudazi, Reza

To be published in: ACS ES&T Engineering

DOI to publisher's version: 10.1021/acsestengg.4c00033

Self-assembled nanofiltration membranes with thermo- and pH-responsive behavior

Younes Saadat [1], Seyed Mostafa Tabatabaei [1], Kyungtae Kim [2], Reza Foudazi [1*]

[1] *School of Sustainable Chemical, Biological and Materials Engineering, The University of Oklahoma, Norman, OK 73019, USA*

[2] *Materials Physics and Applications Division, Center for Integrated Nanotechnologies, Los Alamos National Laboratory, Los Alamos, NM 87545, USA*

ABSTRACT

We produce controlled nanostructured membranes from crosslinking of self-assembled diacrylated poloxamers. At sufficiently high concentrations, poloxamers form lyotropic liquid crystals (LLCs), such as lamellar (L_α), cubic packing of spherical micelles, and hexagonal packing of rod-like micelles in water (H_1). We use H_1 phase as a template to produce orderly packed nanofibrous membranes. The obtained membrane has a continuous 3D transport pathway and can alter its nanofiltration properties in response to changes in temperature and pH. The formulation includes Pluronic P84-diacrylate (P84DA), a thermoresponsive component that acts as both macromer and structure-directing amphiphile. P84DA facilitates changes in membrane pore size with temperature due to its thermo-responsiveness when is in contact with water. Furthermore, the precursor contains acrylic acid (AAc) as the charged component, which upon copolymerization with P84DA, not only enables ion separation through Donnan exclusion, but also imparts pH-responsive behavior for the separation of ionic species. We show that the nanofiltration membrane has separation properties adjustable with temperature and pH with exceptional resistance to fouling by various solutes due to its highly hydrophilic surface. Furthermore, the membrane shows an outstanding sulfate over chloride ion selectivity, which is a requirement for salt fractionation applications. Deducted from separate experiments, the ideal chloride/sulfate selectivity for magnesium cation is about 2.38 at low ionic strengths. This study is done on a model system to show the capability of incorporating pH-responsiveness in LLC templated membranes, in which the pH-responsive range can be designed by changing the charged groups of comonomer in the formulation.

Keywords: *Nanofiltration, Membranes, Stimuli-responsive, Mesophases, Self-assembly*

[*] Corresponding author. Email: rfoudazi@ou.edu.

1. INTRODUCTION

In today's world, the significance of nanofiltration (NF) membranes is rising due to their utilization in a variety of applications, including but not limited to water softening,[1] industrial wastewater remediation,[2] salt fractionation in water streams,[3,4] organic solvents nanofiltration,[5] and bio-separation.[6] Porous NF membranes facilitate the separation process through three mechanisms: size-exclusion, solution diffusion, and electrostatic interaction (also known as Donnan exclusion).[4] The common methods used to produce NF membranes with the ability to separate dissolved salts and molecular solutes at the 1 nm length scale are non-solvent induced phase separation (NIPS)[7,8] and interfacial polymerization.[9–11] Although these methods offer certain benefits, they also come with some drawbacks. NIPS has limited control over membrane pore size distribution, and the process is also environmentally concerning due to the substantial amount of organic solvents required (up to 70% by volume).[12] The disadvantages of interfacial polymerization include limitations in the choice of monomers, variations in membrane properties (e.g., pore size, thickness, and surface morphology) due to the complex nature of the process, and susceptibility to fouling.[13,14]

Lyotropic liquid crystal (LLC) templating is an alternative approach which can address these challenges. To provide a brief background, LLCs are mesoscopic structures that exhibit long-range periodic order ranging from 2 to 50 nm, formed via self-assembly of amphiphiles in selective solvents.[15–20] Out of the various nanostructures available for LLCs, the most frequently utilized ones for synthesizing NF membranes are normal hexagonal (H_1)[5,13,17] and normal bicontinuous cubic (Q_1).[21–24] Although both structures offer the desirable features of a 3D-continuous transport path without requiring structural alignment, H_1 is particularly attractive as it forms more frequently and is available in a wider range of compositions compared to Q_1, making it a more ideal option for membrane applications.[17] A significant achievement in the field was demonstrated by Osuji and coworkers,[5,13,17] where they successfully synthesized H_1-structured NF membranes with an effective pore size of ~1 nm, molecular weight cutoff (MWCO) of ~300 Da, and permeability of ~20 liters m^{-2} $hour^{-1}$ bar^{-1}. Notably, these membranes outperformed commercially available NF membranes like Dow FILMTEC NF90-400, which typically exhibit a permeability of 10 to 15 liters m^{-2} $hour^{-1}$ bar^{-1}.[12]

The incorporation of stimuli-responsiveness into membranes can offer new opportunities for applications by enabling dynamic selectivity and permeability,[25–30] and enhanced cleaning of a

fouled membrane.[25,26,31] While there are some reports on the production of stimuli-responsive ultrafiltration (UF) membranes by using LLC templates,[26,32] there are only a few studies in the literature available on the synthesis of stimuli-responsive NF membranes from LLC templates. Zhu et al.[33] reported an LLC-based sodium selective isoporous membrane, which offered ion conductive channels lined with carboxylate groups. Other than high Na^+/K^+ selectivity due to the interactions of ions and carboxylate groups, this membrane also exhibited pH responsiveness allowing for charge-governed ion transport. Li et al. synthesized a pH- and light-responsive nanoporous polymer with a pore size of about 1 nm, but the potential of the polymerized LLC as an NF membrane was not evaluated in their study.[34] By incorporating pH responsiveness to LLC templated membranes, we could extend the functionalities of such membranes beyond narrow pore size distribution, increased fouling resistance, and enhanced backwashing. Furthermore, this incorporation is experimentally simple in LLC-based membranes as a comonomer with charged responsive group is copolymerized to the network simultaneously and no additional step is required. In contrast, other methods like surface modification and grafting, which are used for NIPS and thin-film composite (TFC) membranes, usually have more complex chemistry[35] and are time consuming.[36]

The advantages of thermoresponsive membranes have been thoroughly discussed in our previously published papers.[26,32] Other than selective separation of solutes, cleaning process using the thermoresponsive property is one of the main advantages. NIPS and TFC nanofiltration membranes with pH-responsiveness have also been studied in the literature for a wide range of applications. For example, Himstedt et al. developed pH-responsive NF membranes by incorporating poly(acrylic acid) for the selective separation of glucose and sucrose, leveraging pH-induced changes in membrane properties to enhance filtration performance in food and dairy industries.[35,37] In another study, carboxybetaine was incorporated to produce NF membranes that are capable of separating organics/inorganic salts mixtures and divalent/monovalent ions systems by adjusting the pH of the feeding solution.[38] Setiawan et al. demonstrated the development of pH-tunable and pH-responsive polybenzimidazole nanofiltration membranes, showcasing an approach for effective and selective separation of lithium and magnesium ions, which could outperform similar commercial membranes.[39] The applications can go beyond water treatment, for example in separation of biomolecules,[40] water/alcohols separation,[41] and organic solvent nanofiltration.[5]

In the current research, we present the first successful production of H_1-structured stimuli-responsive NF membrane via LLC templating. To create the membrane, we polymerize the LLC from mixture of Pluronic P84-diacrylate (P84DA), 1-butyl-3-methylimidazolium tetrafluoroborate ([BMIM][BF_4]) ionic liquid, acrylic acid (AAc), and 1,6-hexanediol diacrylate (HDDA) by using UV light. After removing the ionic liquid (IL) through washing with water, the resulting polymerized LLC (polyLLC) membrane exhibits a pore size of 2.2 nm. When the polyLLC membrane is heated to 45°C, the pore size increases to 2.6 nm, which leads to an increase in thickness-normalized flux and membrane MWCO from 16 to 31 liters m^{-2} $hour^{-1}$ μm and from 1600 to 2400 Da, respectively. The addition of AAc into the formulation incorporates charge on the pore wall, enabling the membrane to effectively reject dissolved trivalent and divalent salts at neutral and alkaline pH levels. Moreover, highly hydrophilic surface of membrane makes it resistant to fouling from various solutes.

2. EXPERIMENTAL

2.1. Materials

All the chemicals used in this study were purchased from Sigma-Aldrich and were used without any purification unless otherwise noted. The components employed in the synthesis of the polymerizable poloxamer, P84DA, were Pluronic P84 (PEO_{19}−PPO_{43}−PEO_{19}) with an average molecular weight of 4,200 g/mol, anhydrous dichloromethane (≥99.8%), anhydrous toluene (99.8%), triethylamine (99.5%), and acryloyl chloride (97%). The desired LLC was produced by mixing P84DA with [BMIM][BF_4] (≥98%), HDDA (99%; Thermo Scientific Chemicals), AAc (99%), and 1-hydroxycyclohexyl phenyl ketone (HCPK; 99%). For all the experiments, deionized (DI) water with a conductivity of 0.055 μS/cm, which was acquired from EMD Millipore Direct-Q3, was employed.

The performance of the membrane, which includes MWCO, rejection of proteins, salts and dyes, and resistance to fouling, was assessed by filtering various solutes. These solutes comprised of polyethylene glycol (PEG) with molecular weights ranging from 1 to 10 kDa, bovine serum albumin (BSA) in the form of lyophilized powder (≥96%), lysozyme from chicken egg white (lyophilized powder with protein content ≥90%), direct red 23 (DR23) with 30% dye content, direct red 80 (DR80) with 25% dye content, orange G (OG) with 80% dye content, acid fuchsin (AF) with 70% dye content, acid red 1 (AR1; TCI America™), K_3PO_4, Na_3PO_4, Na_2HPO_4,

Na_2SO_4, K_2SO_4, $MgSO_4$, Na_2CO_3, NaH_2PO_4, KNO_3, $MgCl_2$ (Thermo Scientific Chemicals), $CaCl_2$, NaCl (Thermo Scientific Chemicals), KCl, and LiCl (Thermo Scientific Chemicals). Sodium hydroxide (NaOH) and hydrochloric acid (HCl) were used for pH adjustments. The membrane support layer, which was a nonwoven polyester sheet with 2 μm porosity (CraneMat® CU463), was provided by Neenah Filtration. A commercially available Dow FILMTEC NF270-400 (NF270) with a MWCO of 400 Da was utilized to assess the pH-dependent rejection of ionic species and compare it with the performance of the membrane produced in this study.

2.2. Synthesis of P84DA

P84DA was synthesized via a functionalization reaction on P84 following a previously described procedure[32] and a commonly accepted protocol available in the literature.[42,43] The degree of functionalization reaction was evaluated using nuclear magnetic resonance spectroscopy (1H NMR, Varian VNMRS-400 with Probe AutoX-DB-PFG). Further details regarding this analysis can be found in section S1 of the Supplementary Information.

2.3. LLC preparation

To produce the H_1-structured LLC, a mixture of P84DA, [BMIM][BF_4] (containing 1 wt% HCPK with respect to [BMIM][BF_4] as UV initiator), AAc, and HDDA (containing 10 wt% HCPK with respect to HDDA) was prepared at a weight ratio of P84DA/[BMIM][BF_4]/AAc/HDDA = 48.8/48.8/0.5/1.9. The mixture was repeatedly hand-mixed and centrifuged at 11,000 rpm for 5 minutes in a 50 mL centrifugal tube until a transparent gel was obtained. The chemical structure of the components utilized for mesophase preparation is depicted in Fig. 1, and a schematic of the H_1 structure is presented in Fig. 1f.

2.4. LLC and polyLLC characterization

2.4.1. Cross-polarized light microscopy (CPLM)

To assess the birefringence of the H_1-structured sample before and after polymerization, a cross-polarized Nikon microscope (model LABOPHOT2-POL) equipped with a digital camera was utilized. For CPLM analysis, ~0.2 g of the mesophase gel was placed between a glass slide and a glass cover slip. To polymerize the LLC, the sandwiched sample was UV-cured for 40 seconds

using a Uvitron Sunray 600 SM curing system equipped with a 600 W UV flood lamp placed 15 cm above the sample. The structure of the polymerized LLC is schematically illustrated in Fig. 1f.

2.4.2. Small angle X-ray scattering (SAXS)

SAXS was used to evaluate the structure of samples and determine the formulation that exhibits the desired H_1 structure. Quartz capillary tubes with a nominal diameter of 1.5 mm (Charles Supper Company, Natick, MA) were used for sample preparation following the procedure described in our previous work.[32] 2D scattering patterns were acquired using a Bruker Nanostar X-ray scattering system equipped with a monochromatic Cu Kα radiation source (X-ray wavelength of 1.541 Å) and were azimuthally averaged to obtain 1D scattering profiles. SAXS analysis was carried out at various temperatures for LLC gels and water-swollen polyLLCs to investigate potential structural changes upon temperature variation. Moreover, polyLLCs swollen by water at pH of 4, 6 and 9 were analyzed using SAXS to examine any probable structural changes upon pH change.

2.4.3. Differential scanning calorimetry (DSC)

Differential scanning calorimetry (DSC) was employed to examine the thermal properties of various samples, including pure P84DA, water-swollen polyLLC, and dried polyLLC (the water-swollen polyLLC sample was dried under vacuum for at least 72 hours). ~10 mg of each sample was placed in an aluminum pan (PerkinElmer, Inc.) and was hermetically sealed. Thermal analysis was performed using a calorimeter (Q2500, TA Instruments, New Castle, DE) operated at a heating/cooling rate of 1 °C/min. The heating/cooling cycle between 0 and 60 °C was repeated twice and the second cycle was used for analysis after erasing the thermal history of the samples.

2.4.4. Swelling characteristics of the polyLLC

A 500 μm thick LLC film was sandwiched between two glass plates and photopolymerized at room temperature. The resulting polymer film was washed multiple times with water and then dried under vacuum. From this film, samples with approximately 2 cm × 2 cm size were cut for water uptake experiments. Each sample was immersed in an excess of DI water at the desired temperature (with a precision of ±0.1 °C) until it reached equilibrium swelling. The swollen samples were then removed from the water and any excess water on the surface was removed with a paper towel. The water uptake (swelling capacity) was determined by using the weight of the dry state (W_0) and the swollen state (W_t), according to the following equation:

$$Swelling\ Capacity = \frac{W_t - W_0}{W_0} \times 100 \quad (1)$$

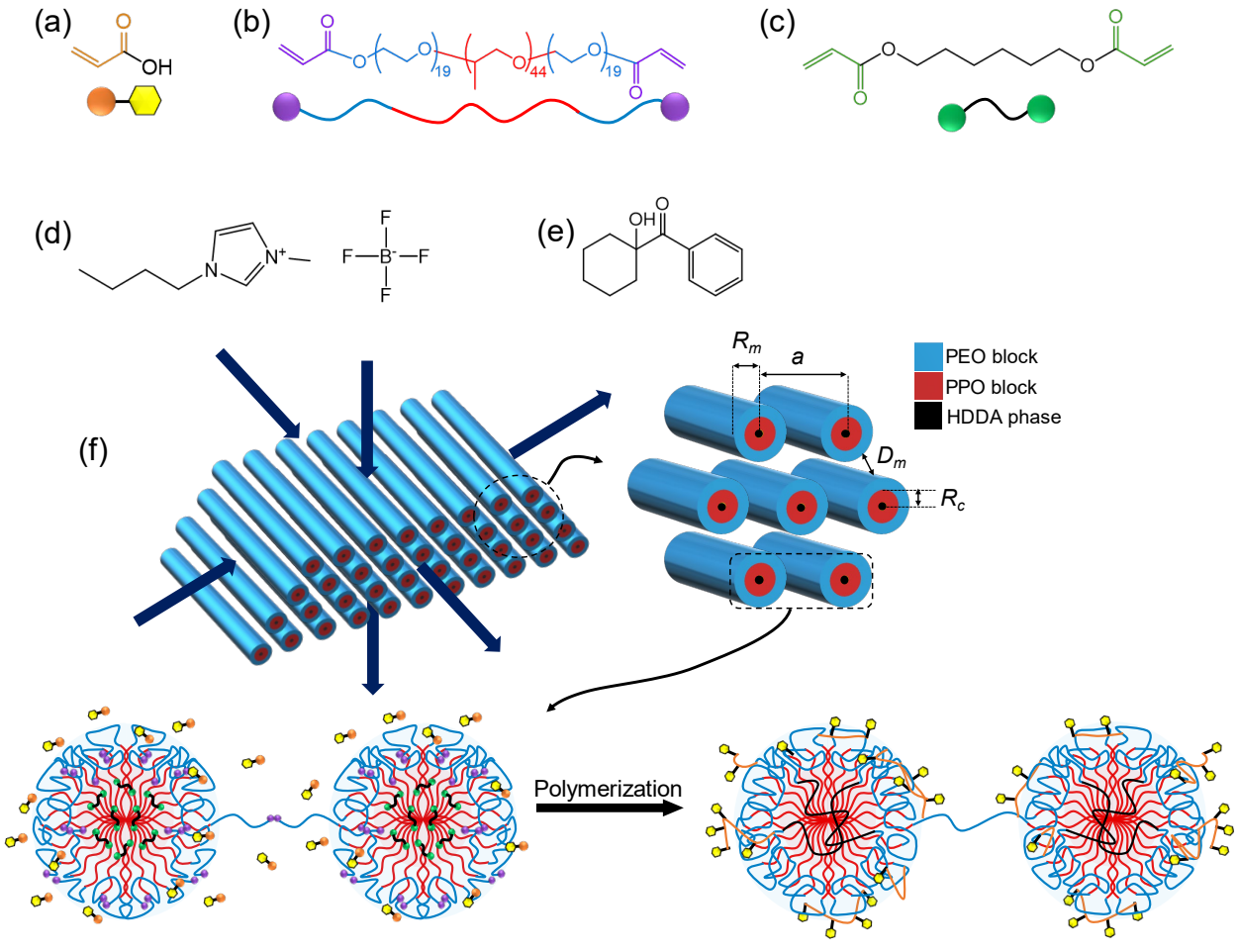

Fig. 1. Molecular structure of (a) AAc, (b) P84DA, (c) HDDA, (d) [BMIM][BF_4], and (e) HCPK. Schematic illustrations of AAc, P84DA, and HDDA have also been shown in panel (a), (b), and (c), respectively. (f) A schematic depiction of an H_1-structured LLC, showing 3D transport pathways, obtained by blending various components, wherein the micelles are enveloped by a mixture of [BMIM][BF_4] and AAc. Important structural parameters have also been shown in the schematic. The apolar domain consists of PPO block and HDDA. A chemically bound polymer network is formed from reaction of acrylate groups of P84DA, HDDA, and AAc. To achieve a well-integrated H_1-structured membrane, it is crucial to have intermicellar bridges, which are formed from reaction of acrylate groups of extended PEO blocks.[17]

The kinetics of thermal response was investigated by transferring the swollen sample from a water bath at 25 °C to one maintained at 45 °C, followed by time-course monitoring the water uptake at different intervals. To confirm the reversibility of the response, the sample was subjected to several cycles of sequential environmental changes (i.e., transferred back and forth between 25 and 45 °C water baths), and the swelling capacity was measured after each change.

To evaluate the salt-dependent swelling behavior of polyLLC, the polymer was swollen in aqueous solutions of K_2SO_4 at different ionic strengths (1, 5, 10, 50, and 100 mM) at 25 and 45 °C. Additionally, the swelling capacity of polyLLC was measured at different pH values ranging from 3 to 9 to investigate the pH effect on its swelling behavior.

Water uptake measurements were performed on a minimum of three samples, and the average value along with the standard deviation is presented.

2.5. Manufacturing of the supported polyLLC membrane

As stated in our previous research,[32] these LLC formulations have the ability to undergo structural changes when heated (see Fig. S2 for SAXS analysis), resulting in a decrease in their viscosity. This property enables the application of the mesophase onto a polyester support sheet using knife coating, followed by UV polymerization to produce a polyLLC membrane supported on the sheet. Further information regarding the membrane fabrication process is available in our prior publication.[32] The thickness of the polyLLC coated layer was determined using Scanning Electron Microscopy (SEM, ThermoFisher Quattro S field emission environmental SEM).

To replace the IL with water, the manufactured membrane was submerged in water for a minimum of one week before being tested.

2.6. Analysis of the polyLLC membrane performance

2.6.1. Water flux and permeability

The Sterlitech HP4750 high-pressure stirred cell (a dead-end filtration system) was employed to assess the performance of the membrane, with an effective area of 14.6 cm^2, operating under stirring at 750 rpm using a magnetic stirrer and a pressure of 30 psi (2.07×10^5 Pa). The thickness-normalized flux of the membrane, reported as liters m^{-2} $hour^{-1}$ μm, was measured at both 25 and 45 °C. To measure the flux at an elevated temperature, the filtration cell containing the membrane was placed in a water bath set to 45 ± 0.1 °C. The permeate collection was initiated only after

verifying the isothermal conditions at the membrane level and obtaining a stable flux. All measurements were conducted on three separate membranes.

Permeability of the membrane was calculated based on Darcy's law.[44] The parameters in this equation are Q (flow rate), μ (viscosity), A (membrane area), ΔP (pressure difference across the membrane), l (membrane thickness), and κ (Darcy's constant or intrinsic permeability).

$$\frac{\kappa}{l} = \frac{Q\mu}{A\Delta P} \quad (2)$$

We obtained the viscosity of water at both 25 and 45 °C from the literature.[26,45] To eliminate the impact of thickness variation in our assessments, we calculated the thickness-normalized intrinsic permeability because membranes with lower thickness would have higher flux. In other words, according to Darcy's law in membranes and neglecting the non-idealities, multiplication of water flux and thickness of a membrane in the same pressure and temperature is constant.[46] A membrane with higher thickness-normalized flux has a more permeable active layer. Since we are considering the DI water flux here, there is no concentration change that can directly or indirectly affect the membrane resistance according to Darcy's law.[47]

2.6.2. MWCO and membrane rejection performance against proteins, single salts, and dyes

To measure the MWCO, we filtered 1 mg/mL aqueous solutions of PEG with varying molecular weights (ranging from 1 to 10 kDa) using one membrane. For each analysis, we collected at least 5 mL of permeate. In 0.3 mL of the collected permeate, we added 3 mL of a reagent[48] consisting of potassium iodide (2 g) and iodine (1.27 g) in water (100 mL) to be able to measure the concentration of PEG by using UV-Vis spectroscopy. The iodine and iodide ion react together and produce triiodide ions, which react with oxygen atoms of PEG through charge transfer complex formation. Within 15 minutes of sample preparation, we employed UV-Vis spectroscopy (Thermo Scientific™ GENESYS™ UV-Vis Spectrophotometer) to determine the concentration of PEG in the permeate. We utilized the following equation to compute the PEG rejection:

$$r = (1 - \frac{C_p}{C_f}) \times 100 \quad (3)$$

The equation involves three parameters: r (rejection), C_p (solute concentration in the permeate, e.g., PEG), and C_f (solute concentration in the feed). The molecular weight of PEG that showed a rejection of about 90% is considered as the MWCO.[49]

The aqueous solutions of following components were used to evaluate the membrane performance in terms of the rejection of protein, dye, and single salt:

1) BSA and lysozyme proteins with a concentration of 1 mg/ml.
2) DR23, DR80, OG, AF, and AR1 dyes with a concentration of 0.5 mg/ml.
3) K_3PO_4, Na_3PO_4, Na_2HPO_4, Na_2SO_4, K_2SO_4, $MgSO_4$, Na_2CO_3, NaH_2PO_4, KNO_3, $MgCl_2$, $CaCl_2$, NaCl, KCl, and LiCl salts having different ionic strengths (1, 5, 10, 50 and 100 mM).

A fresh membrane was employed for each experiment. To determine the contents of proteins and dyes in the permeate, UV-Vis spectroscopy was utilized. The conductivity measurement via Fisherbrand™ accumet™ XL200 pH/conductivity meter was used to measure the salt concentration in the permeate. Equation 3 was applied to calculate the rejection of various species.

Thermoresponsive properties of the membrane were evaluated at two different temperatures, 25 and 45 °C. To do so, the experiment was first performed at 25 °C and then at 45 °C with the same membrane. The reversibility of the thermoresponsiveness was evaluated by cooling the same membrane back to 25 °C and repeating the rejection experiment. To determine the selectivity of the membrane for ionic species as a function of pH, the rejection of Na_2SO_4, K_2SO_4, $MgSO_4$, OG, AF, and AR1 was measured at different pH values ranging from 3 to 9. For comparison purpose, we evaluated the pH-dependent rejection of OG using a commercially available NF270 membrane as well. The pH of the aqueous solutions was adjusted by HCl and NaOH having 0.1 M concentration.

All the membrane performance experiments were conducted for three individually prepared membranes, and the reported results represent the average value and standard deviation from the three trials.

2.6.3. Contact angle and fouling resistance

The contact angle of the membrane was measured using an optical tensiometer from Biolin Scientific. The fouling resistance of the membrane was evaluated by filtering aqueous dispersions of PEG (10 kDa), BSA, and DR80 at a concentration of 1 mg/mL. The filtration cell was initially filled with approximately 250 mL of solution, and 5-8 mL of permeate was collected every 12 h. The test was conducted over 60 h, and the membrane flux and rejection were measured at 12-h time intervals.

3. RESULTS AND DISCUSSIONS

3.1. Characterization of LLC and polyLLC

The structural analysis of LLC and polyLLC was conducted using CPLM and SAXS. After preparation and screening of several samples, LLC with P84DA/[BMIM][BF_4]/AAc/HDDA 48.8/48.8/0.5/1.9 w/w/w/w composition was selected since it has the desired structure before and after polymerization as well as after exchange of IL with water. Anisotropic mesostructures like hexagonal or lamellar show birefringence, which means that they have a refractive index depending on the polarization and propagation direction of light passing through them. The CPLM results (Fig. 2a-c) indicate that the LLC, polyLLC, and water-swollen polyLLC exhibit the birefringent characteristic of hexagonal mesophases, which is a fan-like texture.[16,50] This indicates that the original LLC structure remains intact even after polymerization and solvent exchange. Fig. 2d displays the obtained 1D SAXS profiles, which support the findings from CPLM. The presence of Bragg peaks with $1{:}\sqrt{3}{:}\sqrt{7}$ q/q^* ratios for the LLC is observed in the data, where q represents the scattering vector and q^* represents the primary peak position in each curve. Thus, the LLC has an H_1 structure. Similar Bragg peaks ratios have been reported for LLCs with H_1 structure.[5,13,17] Additionally, the presence of the typical birefringence associated with the H_1 structure and the retention of the distinct SAXS peaks confirm that the structure is preserved following polymerization and solvent exchange (i.e., exchange of IL with water in polyLLC).

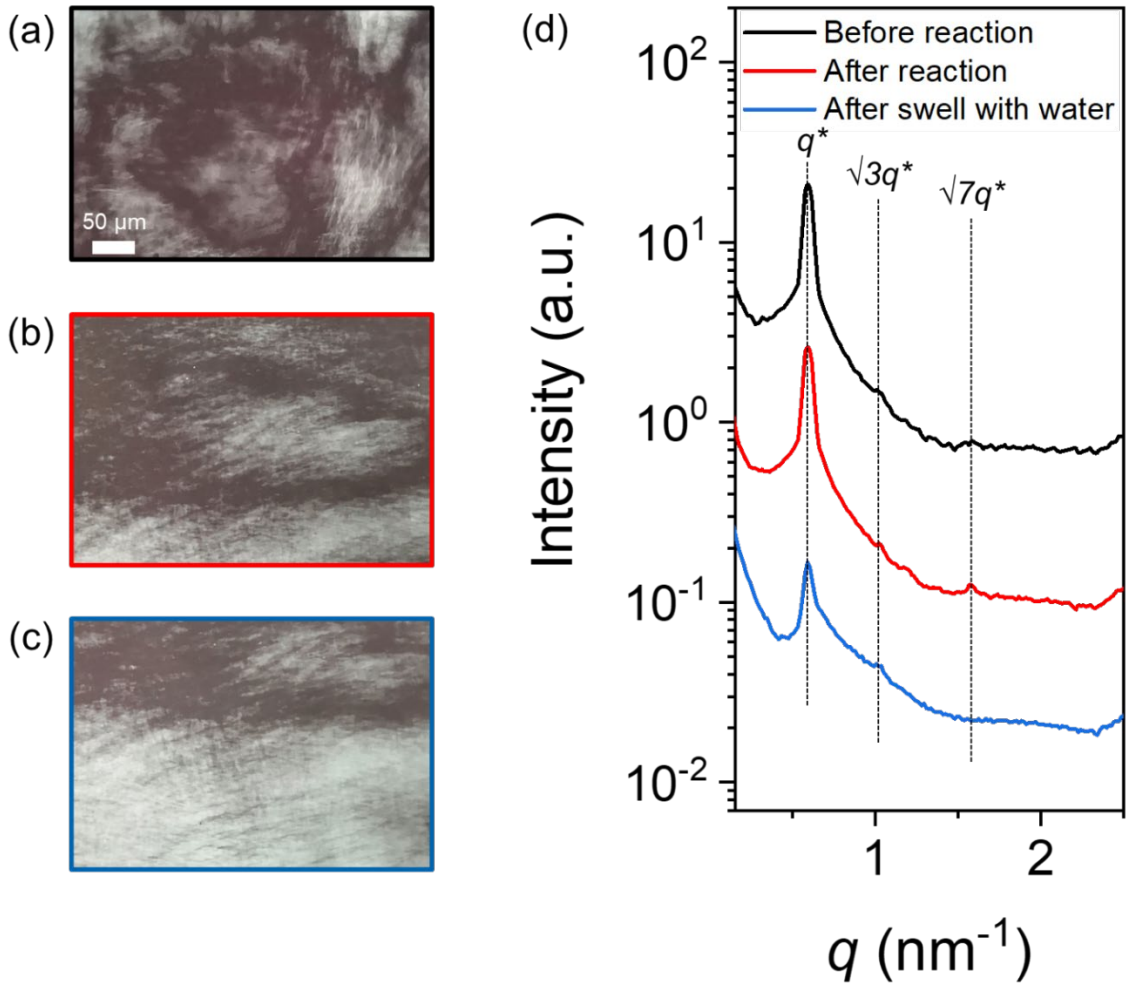

Fig. 2. The images taken using CPLM display the samples in three different stages: (a) their original state (LLC), (b) after undergoing a reaction, and (c) after swelling with water. (d) 1D SAXS profile, in which plots are vertically shifted for clarity.

From the SAXS data, structural parameters such as intermicellar distance (which determines the pore size), lattice parameter, apolar domain size, micelle size, and grain size can be estimated. A schematic representation of these parameters is shown in Fig. 1f. The following equation can be used to calculate the lattice parameter a for hexagonal structure:[51]

$$a = \frac{4\pi}{\sqrt{3}q^*} \quad (4)$$

As discussed in our previous works,[32,52] it is assumed that the solvent (either [BMIM][BF_4]+AAc or water), PEO, PPO, and HDDA are completely segregated and each domain is characterized by a bulk density.[53] It is important to note, however, that in the case of water-swollen samples, the

polymer and water are not entirely segregated, as the polymer network can absorb significant amounts of water. Furthermore, partitioning of the PEO and PPO blocks in the solvent and HDDA phases makes the calculations somewhat imprecise.[54] Nevertheless, we have shown that the this geometric calculation provides a good agreement with the pore size measured from MWCO.[32,44] In this method, the size of the IL or water domain is assumed to be equal to the pore size of the polyLLC membrane.

It is assumed that the apolar domain, with a volume fraction of ϕ, is formed by the HDDA and PPO blocks, while the solvent and PEO block constitute the polar domain that fills the remaining volume (1- ϕ). Therefore, the size of the apolar domain, R_c, is calculated as:[51,55]

$$R_c = a\sqrt{\frac{\sqrt{3}}{2\pi}\phi} \tag{5}$$

The micelle size R_m can be calculated as:[59]

$$R_m = a\sqrt{\frac{\sqrt{3}}{2\pi}(\phi_{Pluronic} + \phi_{HDDA})} \tag{6}$$

In this equation, $\phi_{Pluronic}$ represents the volume fraction of the block copolymer and ϕ_{HDDA} is the volume fraction of the HDDA phase. In our prior work,[32] we have thoroughly explained the derivation of Eq. 5 and Eq. 6.

In the polymerized H_1 structure, the exclusion size of solutes is equivalent to the shortest distance between micelles, which is the same as the intermicellar distance D_m:[54]

$$D_m = a - 2R_m \tag{7}$$

The calculated structural parameters are presented in Table 1. It is evident that the estimated intermicellar distance (pore size) is approximately 2.7 nm for both the LLC and polyLLC samples. However, this value increases to around 4.2 nm for the water-swollen sample at 25 °C and pH 6. The MWCO experiment can be utilized to achieve a more precise measurement of the pore size. Further details regarding the MWCO experiment will be provided in section 3.2.2. As control sample, we have included the calculated parameters for the water-swollen polyLLC at 45 °C and pH 6 in Table 1. Fig. 5 displays the corresponding SAXS data for this specific sample. The calculated data for this particular sample will be discussed in detail in section 3.2.2.

Table 1. Structural parameters for various species determined through calculations using SAXS data.

Sample	q^* (nm^{-1})	ϕ_{PPO} [a]	ϕ_{HDDA}	$\phi_{Pluronic}$	f	a (nm)	R_c (nm)	R_m (nm)	D_m (nm)
LLC	0.59	0.66	0.021	0.53	0.37	12.4	3.9	4.8	2.7
PolyLLC	0.58	0.66	0.021	0.53	0.37	12.5	4.0	4.9	2.7
Water-swollen polyLLC at 25 °C and pH 6	0.60	0.66	0.014	0.37	0.26[b]	12.0	3.2	3.9	4.2
Water-swollen [c] polyLLC at 45 °C and pH 6	0.60	0.66	0.019	0.48	0.33[b]	12.0	3.6	4.4	3.1

[a] The volume fraction of the PPO block in the Pluronic block copolymer is denoted as ϕ_{PPO}.

[b] The volume fraction of the apolar domain in the water-swollen polyLLC was determined by considering the swelling capacity of the polymer at 25 °C and 45 °C, which corresponded to 160% and 100% respectively, as shown in Fig. 4a.

[c] Fig. 5 presents the SAXS data for the water-swollen polyLLC at temperature of 45 °C and pH 6.

DSC was used to analyze the thermoresponsiveness of the water-swollen polyLLC in comparison to pure P84DA and dried polyLLC as control samples. The obtained results are shown in Fig. 3. A thermal transition in 5–32 °C range is seen for the water-swollen polyLLC due to the lower critical solution temperature (LCST) of the poloxamer in water.[56,57] In other words, since dried polyLLC does not show any peak in 5–32 °C range, we conclude that the peak observed for water-swollen polyLLC in this range is due to the LCST and not melting point of PEO block. When the temperature reaches the LCST, the PPO block undergoes a significant increase in hydrophobicity, leading to a reduced water solubility of the block copolymer.[58] On the other hand, pure P84DA exhibits a melting point within the 20–47 °C range, which can be attributed to the melting of the crystalline regions created by the PEO block.[59] We can infer that the formation of polyLLC inhibits the crystallization of the PEO block since dried polyLLC does not exhibit any thermal transition, including melting, crystallization, and LCST transitions. Therefore, the thermal response observed in the water-swollen polyLLC can be attributed to the LCST of the block copolymer surfactant in water.

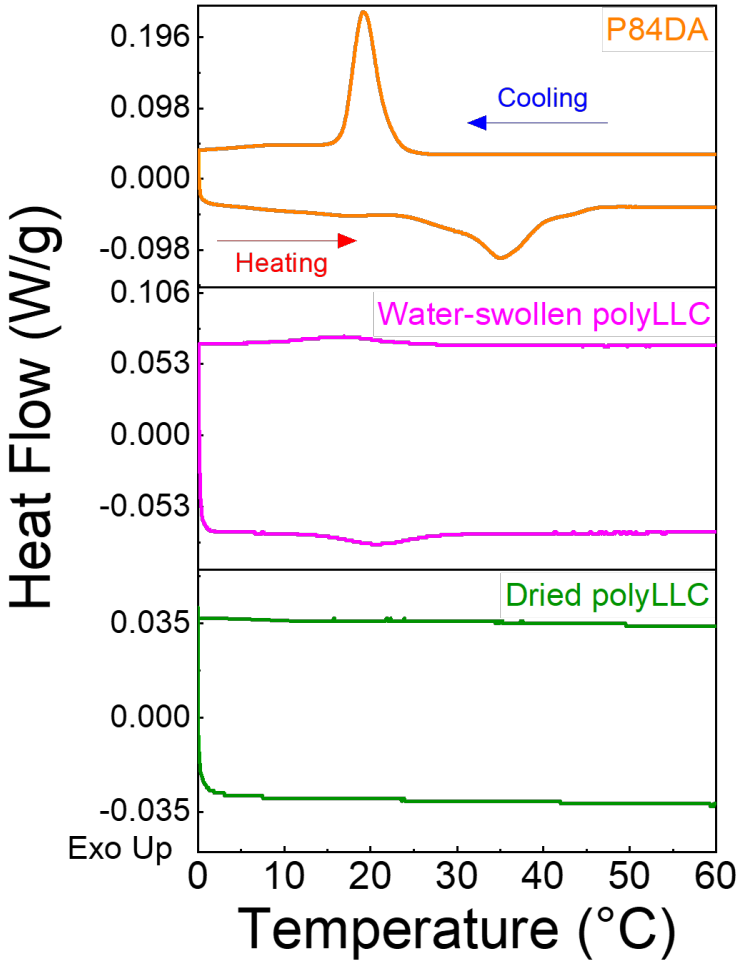

Fig. 3. The DSC data for pure P84DA, water-swollen polyLLC, and dried polyLLC.

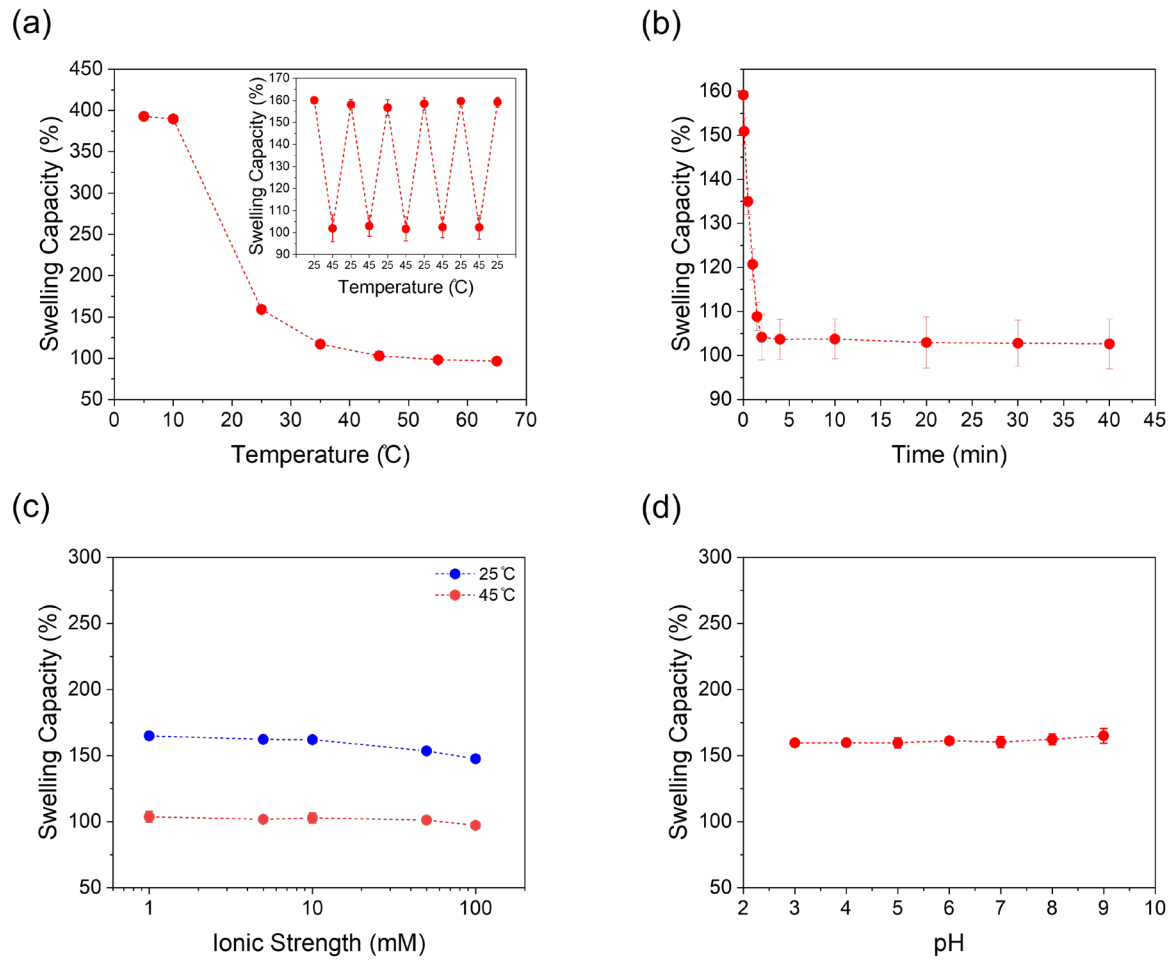

Fig. 4. (a) Variation of polyLLC swelling capacity with temperature (reversibility of the polyLLC thermoresponsiveness is shown as inset). (b) Kinetics of thermal response when the temperature changes from 25 to 45 °C. (c) Changes in swelling capacity with ionic strength at 25 and 45 °C. (d) Variation of the swelling capacity with pH.

The swelling capacity analysis of the polyLLC sample (using pieces with dimensions of approximately 2 cm × 2 cm and a thickness of 500 µm) is shown in Fig. 4. The swelling capacity decreases from around 390% to approximately 100% upon heating the samples from 5 to 45 °C as a result of the LCST of the polymer, in agreement with the DSC measurements. Moreover, our analysis indicates that the thermal response is rapid, occurring within 5 minutes, and fully reversible throughout several heating-cooling cycles. In our earlier study,[32] we found that polyLLCs without AAc exhibited a swelling capacity of 600% at 5 °C, which decreased to 120% when the temperature was raised to 45 °C. The reduction in swelling capacity upon the addition of AAc to the formulation can be considered as a direct effect of inclusion of this specie in the

chemically cross-linked polymer network. It is expected that the copolymerized acrylic acid makes the system more hydrophilic due to the ionization of carboxylate groups, which would result in higher water uptake.[60,61] In addition, carboxylate groups increase the osmotic pressure, which leads to higher swelling capacity.[62] Therefore, the observed decrease in the swelling capacity of polyLLC with acrylic acid comonomer can be attributed to the increased cross-link density of the system, induced by enhanced reactive sites in LLC precursor.

We evaluated the swelling capacity at different pH values and ionic strengths. The ionic strength was altered by using different contents of K_2SO_4. Fig. 4c demonstrates that the polyLLC still exhibits thermoresponsiveness, albeit with a slightly reduced swelling capacity and extent of thermal response (change in swelling capacity upon heating from 25 to 45 °C) at higher salt concentrations. This reduction in swelling capacity is a well-known phenomenon that has been observed in hydrogels when exposed to high salt concentrations. This is due to the high osmotic pressure in the saline water, which causes water to be desorbed from the hydrogel.[63] Additionally, there are no significant changes in swelling capacity at 25 °C when the pH is altered from 3 to 9 (Fig. 4d).

CPLM and SAXS were employed to investigate the impact of temperature and pH on the structural changes of the water-swollen polymer (Fig. 5). The structure of the polymer remains unaffected by changes in pH, as evidenced by the consistent CPLM and SAXS results obtained at various pH values. However, irrespective of the pH values, the results indicate that when the polymer is cooled to 10 °C, it exhibits a weakly ordered structure. This is evident from the absence of any discernible texture in CPLM and the presence of very weak peaks (or almost no peaks) in SAXS. This finding is aligned with our recently published research[32] and can be attributed to the disruption of PEO and PPO segregation within the water domain. This disruption occurs due to the increased miscibility of PEO and PPO with water, which is a result of PPO becoming hydrophilic at temperatures below LCST of the poloxamer.[26,58] Under such condition, the micelles adhere to each other because of significant swelling with water, leading to the formation of a weakly porous polymer that lacks any noticeable structure. Such structural alteration is reversible via deswelling the polymer upon heating it to 65 °C, as confirmed by the reappearance of texture in CPLM and the emergence of strong H_1 Bragg peaks in the SAXS profile.

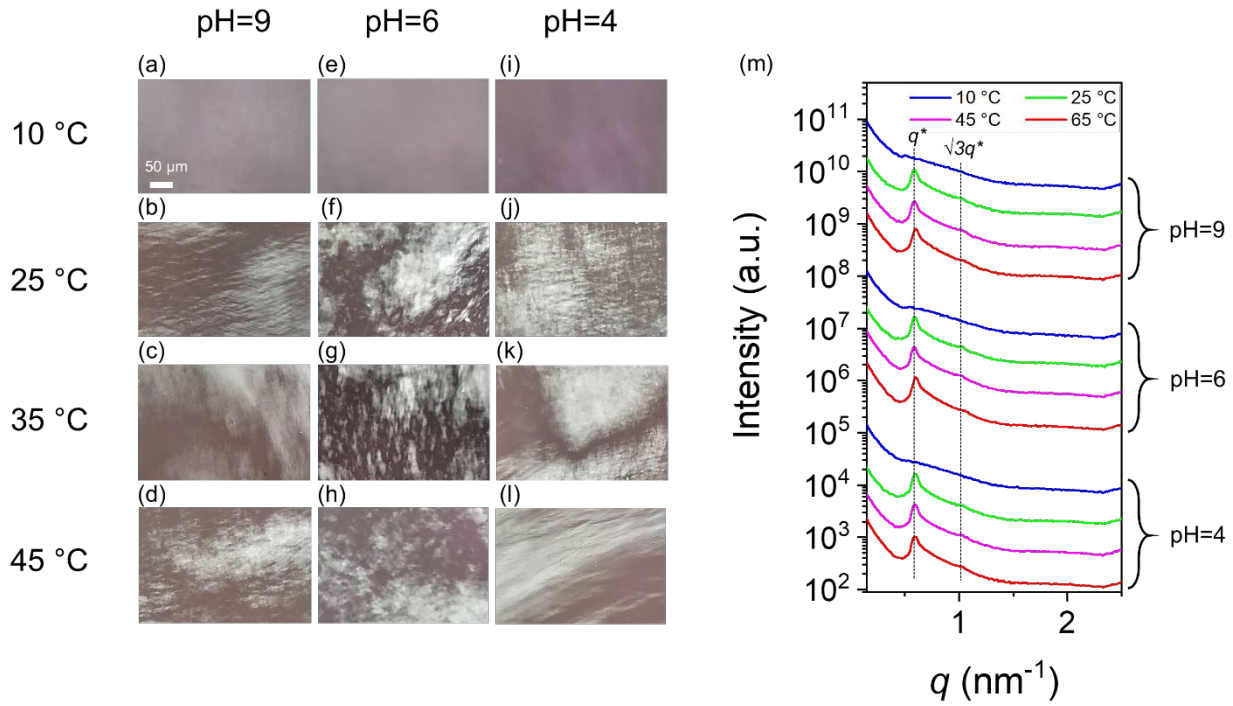

Fig. 5. (a-l) CPLM images of water-swollen polyLLC at temperature of (a, e, i) 10, (b, f, j) 25, (c, g, k) 45, and (d, h, l) 65 °C and at pH of (a-d) 9, (e-h) 6, and (i-l) 4. (m) 1D SAXS profile of the water-swollen polyLLC at different temperatures and pH values. The plots are vertically shifted for clarity.

3.2. Analysis of the polyLLC membrane performance

We have demonstrated the fabrication of an H_1-structured membrane on a polyester support layer by applying a knife coating technique followed by UV curing.[32] The same technique was employed to create the membrane discussed in the present study. The circular cut and typical cross-sectional SEM image of the supported membrane are depicted in Fig. 6a and b, respectively. Based on image analysis, it can be determined that the membrane thickness is in 20–60 µm range with an average thickness of ~40 µm. Consequently, all membrane flux data are normalized by this average thickness to unit of liters m^{-2} $hour^{-1}$ µm.

The performance of the polyLLC membrane is assessed through various tests, and the ensuing sections detail the findings obtained from these tests.

3.2.1. Water flux and permeability

Fig. 6 shows the measurement of membrane flux and permeability in multiple heating-cooling cycles at 25 and 45 °C. The obtained results indicate that both parameters increase and decrease reversibly upon heating and cooling, respectively. As shown in our previous work,[32] commercially

available non-thermoresponsive membranes lack this behavior, which further confirms the thermoresponsiveness of the polyLLC membrane. Notably, the membrane containing AAc exhibits lower permeability than the one without AAc reported in our previous work,[32] suggesting smaller pore sizes due to the incorporation of this species. It is important to note that the membrane created in this study exhibits lower flux when compared to commercially available membranes with a similar pore size. However, this is probably due to the differences in active layer thickness. Higher permeability in the same pore size and same active layer thickness is an expected characteristic of LLC-templated membranes because of their higher and more uniform porosity.[5] In other words, the produced membrane in this work has much thicker active layer thickness than typical NIPS and TFC membranes with ~ 100-200 nm active layer thickness. To tackle this issue, we are currently exploring the possibility of reducing the thickness of the active layer to less than 1 μm using different casting methods (e.g., spin coating), as the common practice reported in the literature.[5,13]

The fabricated membrane in this study is also compared with the well-known commercial membrane, NF270. Our membrane exhibits much lower permeability which is about 0.18 $Lm^{-2}h^{-1}bar^{-1}$, while NF270's permeability has been reported to be more than 10 $Lm^{-2}h^{-1}bar^{-1}$ in the literature.[64,65] We measure the permeability of NF270 membranes by using the same procedure and filtration cell, resulting in a value of 6.5 $Lm^{-2}h^{-1}bar^{-1}$. As discussed earlier, high permeability of NF270 membrane is due to its thin active layer in the range of 150-200 nm.[64] According to Himstedt et al.,[35] NF270 flux is ~70 and ~30 $Lm^{-2}h^{-1}$ at ~5 and ~2 bar at 25 ℃, respectively. Even at 5 bar, the thickness-normalized flux of NF270 would be about 12 $Lm^{-2}h^{-1}\mu m$, which is lower than that of LLC-templated NF membranes at 25 ℃. The thickness-normalized flux for NF270 at ~30 psi, tested in this study, decreases to ~5 $Lm^{-2}h^{-1}\mu m$. These results show the potential of developed LLC templated membrane since it can offer higher operational permeability if proper casting method like spin coating is used.

3.2.2. MWCO, protein, single salt and dye rejection measurements

A fresh membrane was used to conduct the MWCO experiment at 25 °C, followed by conducting the same experiment at 45 °C using the same membrane. To assess the reversibility of the thermal response, the membrane was subsequently cooled down to 25 °C and the MWCO measurement was repeated. The MWCO data, which usually exhibits a sigmoidal trend, was fitted by using the Boltzmann sigmoidal equation, Eq. (9). This equation includes four parameters, namely A_1, A_2, x_0,

and *m*, which correspond to the initial value, final value, center value, and slope at the midpoint, respectively.

$$y = A_2 + \frac{(A_1 - A_2)}{1 + e^{\frac{(x - x_0)}{m}}} \quad (9)$$

As depicted in Fig. 6, the MWCO of the membrane can be altered reversibly from 1600 to 2400 Da by increasing the temperature from 25 to 45 °C. Hernández et al.[66] suggested following equation from regression of MWCO against the hydrodynamic radius of PEG:

$$Pore\,size = 0.12254 \times MWCO^{0.3931} \quad (10)$$

By considering the obtained MWCO values, therefore, an increase in temperature from 25 to 45 °C results in a change in pore size (i.e., pore diameter) from 2.2 to 2.6 nm which is around 18%. The obtained pore sizes are smaller than the ones obtained for polyLLC membrane without AAc in our previous work (2.5 and 3.2 nm at 25 and 45 °C, respectively),[32] which correlates with the permeability results.[32] Additionally, the hydrodynamic radius of PEG within the investigated range of molecular weights (1–10 kDa) displays insignificant changes upon being heated from 25 to 45 °C.[67,68] Thus, the temperature-dependent MWCO of the polyLLC membrane can be attributed to its thermoresponsive nature. As previously reported,[32] non-thermoresponsive commercial UF and NF membranes with comparable pore size do not show alterations in MWCO upon increasing temperature. Dang et al. showed about 15% increase in NF270 membranes pore size by changing the temperature 20 to 40℃.[69] However, the reversibility of this change has not been verified.

The estimated pore size from MWCO analysis at 25 °C (2.2 nm) is smaller than the calculated intermicellar distance of 4.2 nm (see Table 1) determined from SAXS data of the water-swollen sample at the same temperature. A similar deviation is observed at 45 °C, with estimated pore sizes of 2.6 nm compared to the intermicellar distance of 3.1 nm. One reason for the difference is the assumptions made in our calculations based on SAXS data, specially complete segregation of water and the polymer, with water existing only within the pores. In other words, a significant portion of water is trapped between the polymer chains and is released when the membrane is heated, due to the LCST of the polymer. However, the role of this factor is not significant at 45 °C where most of the trapped water within polymer chains has already been released and water is mainly present in the pores. Therefore, there must be an additional factor contributing to this discrepancy. In our previous work,[32] where we used a formulation without AAc, we observed that

the discrepancies in pore size estimation based on MWCO and SAXS were resolved by heating the polymer to 45 °C. This suggests that the copolymerized AAc in the polymer network could be the other factor contributing to water holdup within polymer chains at 45 °C.

Fig. 6 presents the rejection of BSA, lysozyme, DR23, and DR80 for further evaluation of the thermoresponsiveness of the produced membrane. A rejection of over ~85% is observed for BSA and lysozyme, with no significant variation in rejection upon changing temperature. This can be attributed to their large molecular size (~7 nm for BSA[70] and ~3.2 nm for lysozyme[17]), which surpasses the pore size of the membrane at various temperatures.

Fig. 6 illustrates that the membrane rejects over 90% of DR23 and DR80 at 25 °C. It is well-known that these dyes, which have a molecular size of ~1 nm, can form clusters larger than 1 nm in water,[71] As such, the synthesized polyLLC membrane can efficiently reject them at 25 °C. Due to the passage of dye clusters upon increasing the temperature to 45 °C, the rejection of DR23 and DR80 decreases to less than 80% and 85%, respectively. The temperature-dependent changes in the rejection of these dyes are less significant compared to the membrane without AAc in its formulation,[32] which is attributed to the smaller pore size of the membrane containing AAc at 45 °C. The presence of electrostatic repulsions between the COO^- group of copolymerized AAc and the sulfate groups of the dyes may also contribute to the observed differences in rejection values. Overall, the studied polyLLC membranes, with or without AAc in formulation,[32] are capable of expanding their pores at 45 °C, which allows the passage of dye clusters,[71] leading to lower rejection. The reversibility of the change in dye rejection can be observed in Fig. 6.

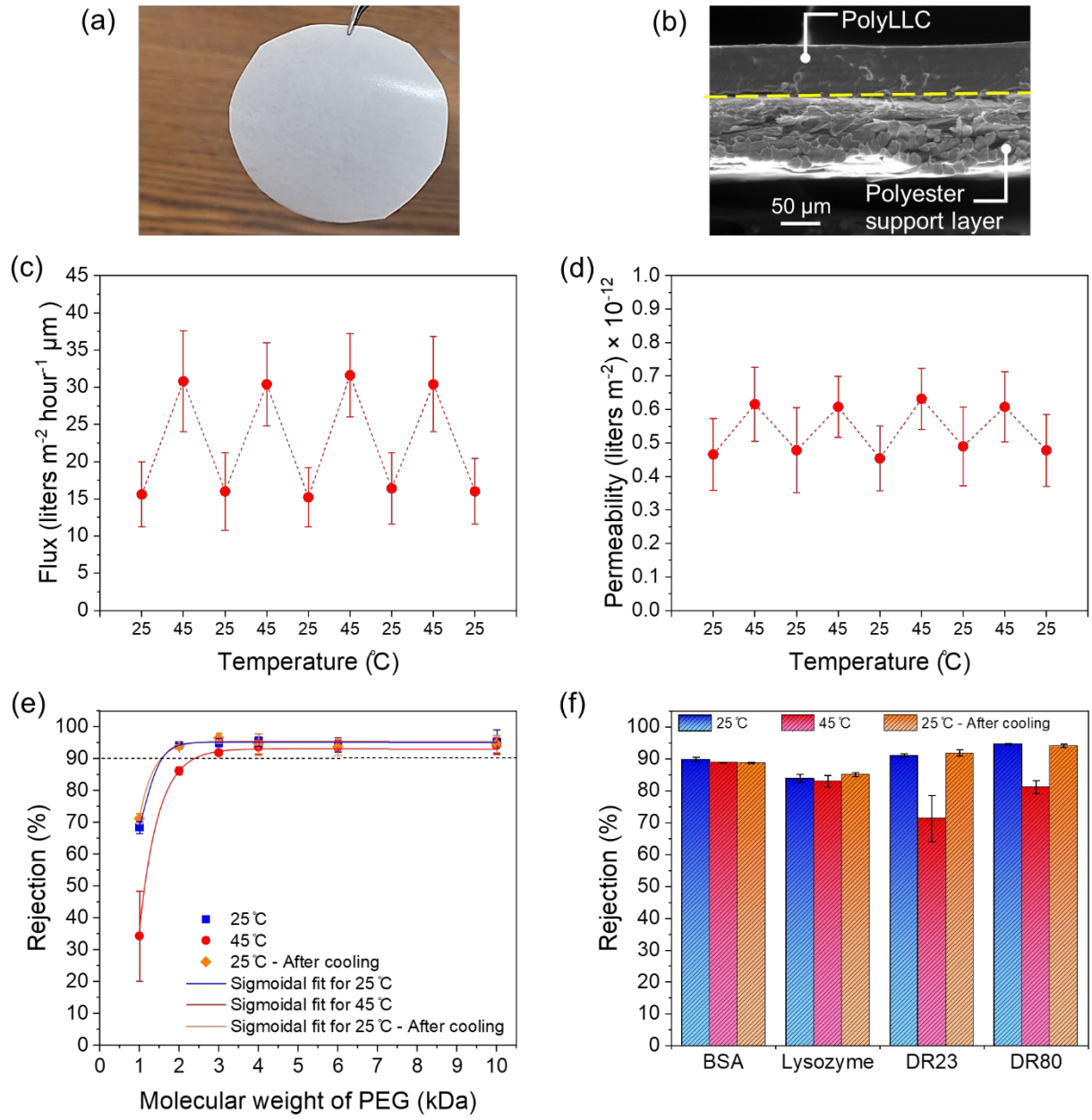

Fig. 6. (a) A supported polyLLC membrane with a circular cut and (b) typical cross-sectional SEM image of the membrane. Cyclical changes of (c) thickness-normalized flux and (d) permeability with changes in temperature. (e) MWCO and (f) rejection of BSA, lysozyme, DR23, and DR80 measured at 25 °C, after increasing the temperature to 45 °C, and after cooling back down to 25 °C. All rejection tests were done at 30 psi.

To evaluate the salt rejection capability of the H_1-structured NF membrane, we performed a single salt rejection experiment using different salts containing monovalent, divalent, and trivalent ions.

Aqueous solutions of these salts (without adjusting the pH) were prepared at ionic strengths of 1, 5, 10, 50, and 100 mM and were passed through the membrane. The results are shown in Fig. 7a, indicating that the membrane exhibits higher rejection for divalent and trivalent species compared to monovalent ones. Additionally, the rejection decreases as the ionic strength is increased.

The separation of ionic species by NF membranes is typically influenced by three primary mechanisms: size-exclusion, solution diffusion, and electrostatic interactions.[4] In membranes where the pore size is larger than the hydrated diameter of the ions, the primary controlling factor in separation is the electrostatic repulsion due to the electrical double layer being larger than the pore diameter.[13] In our membrane, separation mainly occurs based on the electrostatic repulsions between the COO^- group of copolymerized AAc and the anion of the salt. Based on the electroneutrality principle, therefore, the cation of the salt is also rejected to maintain the neutral ionic conditions on both sides of the membrane. Consequently, the rejection is higher for divalent and trivalent species since they induce stronger electrostatic interactions. With an increase in salt content (ionic strength), electrostatic screening reduces the electrical double layer thickness (Debye length), leading to lower rejection. Debye length, κ^{-1}, can be calculated theoretically using following equation:

$$\kappa^{-1} = \sqrt{\frac{\varepsilon_r \varepsilon_0 RT}{2F^2 I}} \tag{11}$$

Where ε_r, ε_0, R, T, F and I are dielectric constant (with a value of 78.5), permittivity of the vacuum (equal to 8.85×10^{-12} C/V.m), gas constant (measuring 8.314 C.V/mol.K), absolute temperature (at 298 K), Faraday constant (at 9.65×10^4 C/mol) and ionic strength of the solution, respectively.[72] By employing this formula, one can determine Debye lengths of 9.6, 4.3, 3, 1.3, and 0.96 nm for ionic strengths of 1, 5, 10, 50, and 100 mM, respectively. When the ionic strength is less than 50 mM, the calculated Debye length surpasses the size of the membrane pores, aligning with the observed higher salt rejection values. Conversely, for ionic strengths of 50 and 100 mM, the Debye length notably diminishes, falling within the range of the membrane pore size, resulting in decreased rejection. It should be noted that this behavior is mainly controlled by the electric exclusion mechanism, which can be engineered by changing the size of head and tail of the surfactant to achieve sub-nanometer pore size.[5]

With an increase in salt content (ionic strength), electrostatic screening reduces the electrical double layer thickness, leading to lower rejection. As shown in the inset of Fig. 7a, $MgSO_4$ exhibits

lower rejection at low ionic strengths compared to the salts containing the same anion. Such behavior can be attributed to the stronger electrostatic screening effect caused by the higher charge density of magnesium ions (more than 10 times) when compared to sodium and potassium cations.[73] Moreover, the membrane exhibits limited rejection for salts containing chloride ion compared to sulfate, which enables the selective separation of anions such as sulfate over chloride. The selectivity can be calculated using the following equation,[37] in which selectivity of higher than 1 shows higher sulfate rejection:

$$\alpha_{Cl^+/SO_4^-} = \frac{{C_{p,Cl^+}}/{C_{f,Cl^+}}}{{C_{p,SO_4^-}}/{C_{f,SO_4^-}}} = \frac{100-r_{Cl^+}}{100-r_{SO_4^-}} \quad (12)$$

Considering magnesium as cation, the selectivity of sulfate over chloride of polyLLC membranes is about 2.38, which is comparable with NF270 selectivity of 3.48 for the same salts (Fig. S3).

To test the pH-dependent rejection capability of the polyLLC membrane for ionic species, we prepared aqueous solutions of Na_2SO_4, K_2SO_4, and $MgSO_4$ with an ionic strength of 5 mM at different pH values and passed them through the membrane. As typical experiment, the permeate flux of K_2SO_4 was also continuously monitored. Fig. 7b demonstrates that the rejection for the tested salts (e.g., Na_2SO_4, K_2SO_4, and $MgSO_4$) is high and steady in neutral and alkaline solutions, but significantly decreases when the pH drops to 4. Moreover, the consistent flux observed at various pH values suggests that the pore size of the membrane does not change with pH. This finding is in agreement with the SAXS data (see Fig. 5), which demonstrates unnoticeable structural variation in the polyLLC at different pH values. Thus, the change in rejection with pH can be attributed to the isoelectric point of COOH of copolymerized AAc, which is approximately 4.5.[74] As a result, when the pH drops below 4, COOH groups on the polymer chains become protonated, leading to weakened electrostatic repulsion and subsequently lower rejection. As a control experiment, the rejection of same salts at different pH was measured using NF270 membranes. Fig. S4 shows that although the rejection changes with pH, there is no clear trend that one can conclude NF270 is a pH responsive membrane.

To further investigate the pH response, we passed aqueous solutions containing 500 ppm of different anionic dyes through the membrane at different pH values (4, 6, and 9). To minimize the effect of size-exclusion by the membrane, dyes including OG, AF, and AR1 were selected for this experiment which have molecular sizes much smaller than the pore size of the membrane. We did not employ DR23 and DR80 in this test as they can be separated by the membrane through size-

586 exclusion. The results obtained from the experiment (Fig. 7d-g) demonstrate that at pH values of
587 6 and 9, a rejection close to 85% is observed for all the dyes. In contrast, when the pH is set at 4,
588 the rejection drops to 6%, 10%, and 30% for AR1, OG, and AF, respectively. As control
589 experiment, we also tested the OG rejection performance of the commercially available NF270
590 membrane at different pH values. Fig. S5 confirms that the rejection of NF270 remains constant
591 regardless of the pH change, as the separation is primarily dependent on size-exclusion due to the
592 smaller pore size of NF270 (~0.8 nm).[75] The outcomes of these experiments verify that the
593 polyLLC membrane has pH-responsive separation of ionic species although it does not experience
594 any structural changes due to the change in pH.
595 To assess whether thermoresponsiveness affects pH-dependent selectivity for ionic species, we
596 conducted rejection experiments for K_2SO_4 while varying both pH and temperature
597 simultaneously. The results (Fig. 7c) demonstrate that the rate of salt rejection remains constant at
598 both tested pH values despite a change in temperature from 25 to 45 °C. This indicates that altering
599 the pore size with temperature within the studied range has negligible effect on the rejection of
600 ionic species driven by electrostatic repulsion. This outcome is somewhat expected as the polyLLC
601 membrane does not reject studied ions by size-exclusion. Furthermore, at the temperature of 45
602 °C, the membrane pore size, which is ~2.6 nm from SAXS measurements and MWCO analysis, is
603 still smaller than the computed Debye length of 4.3 nm for an ionic strength of 5 mM. This
604 observation provides additional confirmation that such pore expansion resulting from the
605 membrane thermal response has negligible impact on the membrane ability to reject ionic species.

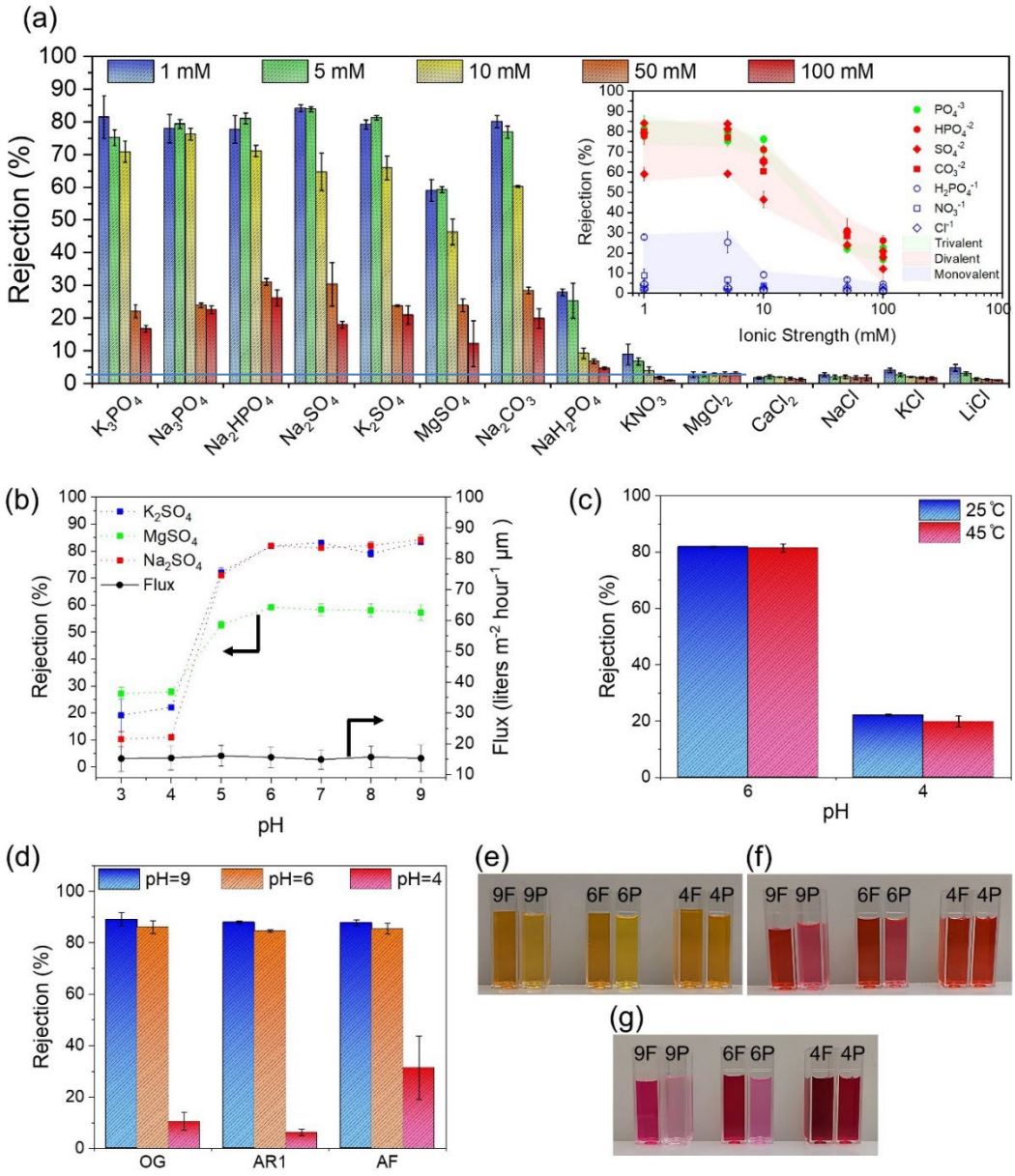

606

607 **Fig. 7.** (a) The results of single salt rejection experiments are presented for different salts and
608 concentrations. The range of rejection observed for different anions is indicated by the shaded areas in the
609 inset. (b) The rejection of different dissolved salts varies with pH. The membrane flux (for K_2SO_4) at
610 different pH values is also presented in the figure. (c) The variation of K_2SO_4 rejection is demonstrated in
611 response to changes in temperature and pH. (d) The pH-dependent rejection for different anionic dyes is
612 displayed. Photos of the feed and permeate at different pH values are provided for (e) OG, (f) AR1, and
613 (g) AF. In these photos, the pH value (9, 6, or 4) is indicated by a number and the letter indicates whether
614 it is feed (F) or permeate (P). It should be noted that the color of the feed for AF changes as the pH is
615 altered since this dye is a pH indicator.

3.2.3. Contact angle and fouling resistance

Fouling is a major challenge in membrane separation processes as it can lead to reduced membrane performance and lifespan. A membrane is particularly susceptible to fouling when it is utilized for filtering feed streams containing species such as proteins, bacteria, and viruses.[76] Increasing the surface hydrophilicity of membranes is a key strategy for mitigating fouling.[77] This occurs because a strongly adhered hydration layer forms on the membrane surface, making it thermodynamically unfavorable for impurities to replace the water molecules. Therefore, we evaluated the surface hydrophilicity of the polyLLC membrane by measuring its water contact angle.[77] The results (Fig. 8a) show an average contact angle of 33° for the polyLLC membrane when swollen at 25 to 45 °C. This suggests that the membrane has a highly hydrophilic surface, which can effectively enhance its resistance to fouling.

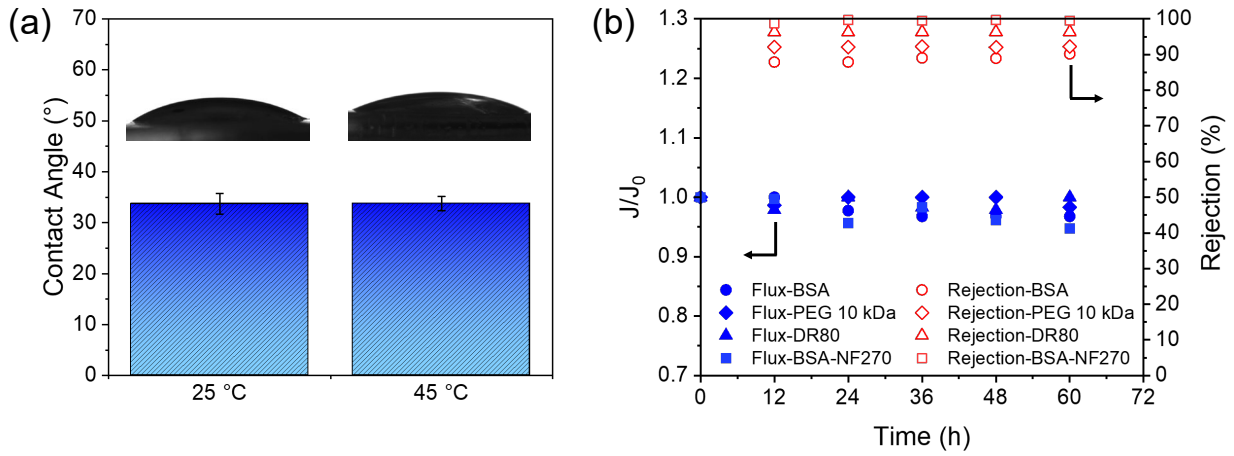

Fig. 8. (a) The contact angle of the polyLLC membrane when swelled with water at 25 and 45 °C. (b) The evolution of the ratio of membrane flux at a given time (J) to the initial flux with DI water ($J_0 \cong$ 0.4 $Lm^{-2}h^{-1}$for polyLLC membranes and 0.35 $Lm^{-2}h^{-1}$ for NF270 membranes) represented by filled symbols and rejection of various solutes represented by open symbols for the polyLLC and NF270 membranes. The first three data sets in the legend of (b) are for polyLLC membrane.

We assessed the fouling resistance using the same procedure outlined in our previous work.[32] In brief, we passed solutions of three different species through the membrane. The filtration setup was kept at 25°C for a period of 60 h while the flux was measured at 12-h intervals. We also monitored the rejection with time to ensure that the membrane was performing consistently. As

demonstrated in Fig. 8b, the membrane flux decreased by less than 4% after 60 h, indicating exceptional resistance to fouling, which can be attributed to the highly hydrophilic surface of the membrane. Comparable findings were reported for polyLLC membrane without AAc in our previous work.[32] Additionally, the constant rejection confirms the reliable and consistent performance of the polyLLC membrane. It is important to note that the membrane is expected to exhibit similar fouling resistance at 45 °C due to its comparable surface hydrophilicity to that observed at 25 °C (with the same contact angle of 33°).

The highest flux decline is observed for rejection of BSA, which is known by its extensive fouling behavior and have been used in many studies to test fouling resistance of membranes.[78,79] As a control experiment, fouling behavior of NF270 for the same concentration of BSA is also monitored. Since the flux of NF270 is higher than polyLLC membrane, the pressure is decreased to reach the same flux, avoiding differences in internal fouling. Overall, NF270 membrane shows higher flux decline than polyLLC membrane. It is worth mentioning that membranes with charged groups have the ability to recover flux after being fouled with BSA. The overall charge of BSA can change from positive to negative by changing the pH from below 4.8 to higher values. Thus, altering the pH of the solution for membranes with charged groups can affect the fouling propensity of the membranes.[80]

We also study the BSA, DR80, and PEG 10 kDa adsorption of the polyLLC after exchanging the IL with water (i.e., water swollen polyLLC sample), which mimics the final membrane condition. The purpose of this measurement is to make sure that rejection of solutes shown in Fig. 8 after 60 h is not due to the adsorption. The amount of polyLLC placed in the solution is 0.3 g/L, which is the same as the ratio of actual membrane in the cell to 250 ml of solution. The concentrations of solutes are the same as used in Fig. 8. As can be seen in Fig. S6, no significant adsorption is observed at 33°C for different solutes after 60 h.

3.3. Mechanisms of thermal and pH response

Fig. 9 illustrates the thermo- and pH-responsiveness mechanisms of the polyLLC membrane. By increasing temperature, the chemically bonded polymer network de-swells, increasing the intermicellar distance, resulting in larger pore sizes. De-swelling is triggered by the LCST of the poloxamer, which makes the PPO block hydrophobic. It is worth noting that such changes in the polymer structure are reversible upon rehydration through cooling the system down to 25 °C.

The polyLLC membrane exhibits pH-responsiveness when the pH of the feed solution is lowered to 4, which is close to the isoelectric point of copolymerized AAc. At this pH, there is a weak electrostatic repulsion between the membrane and the ionic solute due to the fact that COOH group on polymer chains become protonated. Thus, as the membrane separates ionic species primarily based on electrostatic repulsion, the rejection decreases considerably.

4. CONCLUSION

In this research, for the first time, we demonstrate the creation of an NF membrane with thermo- and pH-responsive 3D transport pathway using H_1 structure LLC as the template. This membrane has the capability to modify the separation characteristics in response to changes in temperature and pH. The formulation of the membrane includes P84DA, which acts as both the monomer and structure-directing amphiphile and is also responsible for changes in membrane pore size with temperature. Additionally, AAc was copolymerized with P84DA in the template, thus, facilitating ion separation through Donnan exclusion and imparting pH-responsive behavior. The thickness-normalized flux and membrane MWCO increased from 16 to 31 liters m^{-2} $hour^{-1}$ μm and from 1600 to 2400 Da by raising the temperature from 25 to 45 °C, respectively. Additionally, the membrane demonstrates exceptional resistance to fouling by various solutes due to its highly hydrophilic surface. Furthermore, the developed membrane exhibits excellent performance in removing dissolved trivalent and divalent salts at neutral and alkaline pH levels, and its ion rejection capability can be turned off by lowering the feed pH to 4. We also observe remarkable sulfate ion selectivity over chloride, which is ideal for salt fractionation and selective salt separation applications. Another potential application is separation of uncharged from charged species by leveraging the pH responsiveness capability of these membranes. The main purpose of this study is to present a new framework for membrane fabrication in which LLC templated membranes could offer pH-responsiveness by incorporating the charged comonomer in the precursor. The separation performance can be adjusted by changing charged commoner and surfactant to control the electrical and size exclusion mechanisms, respectively.

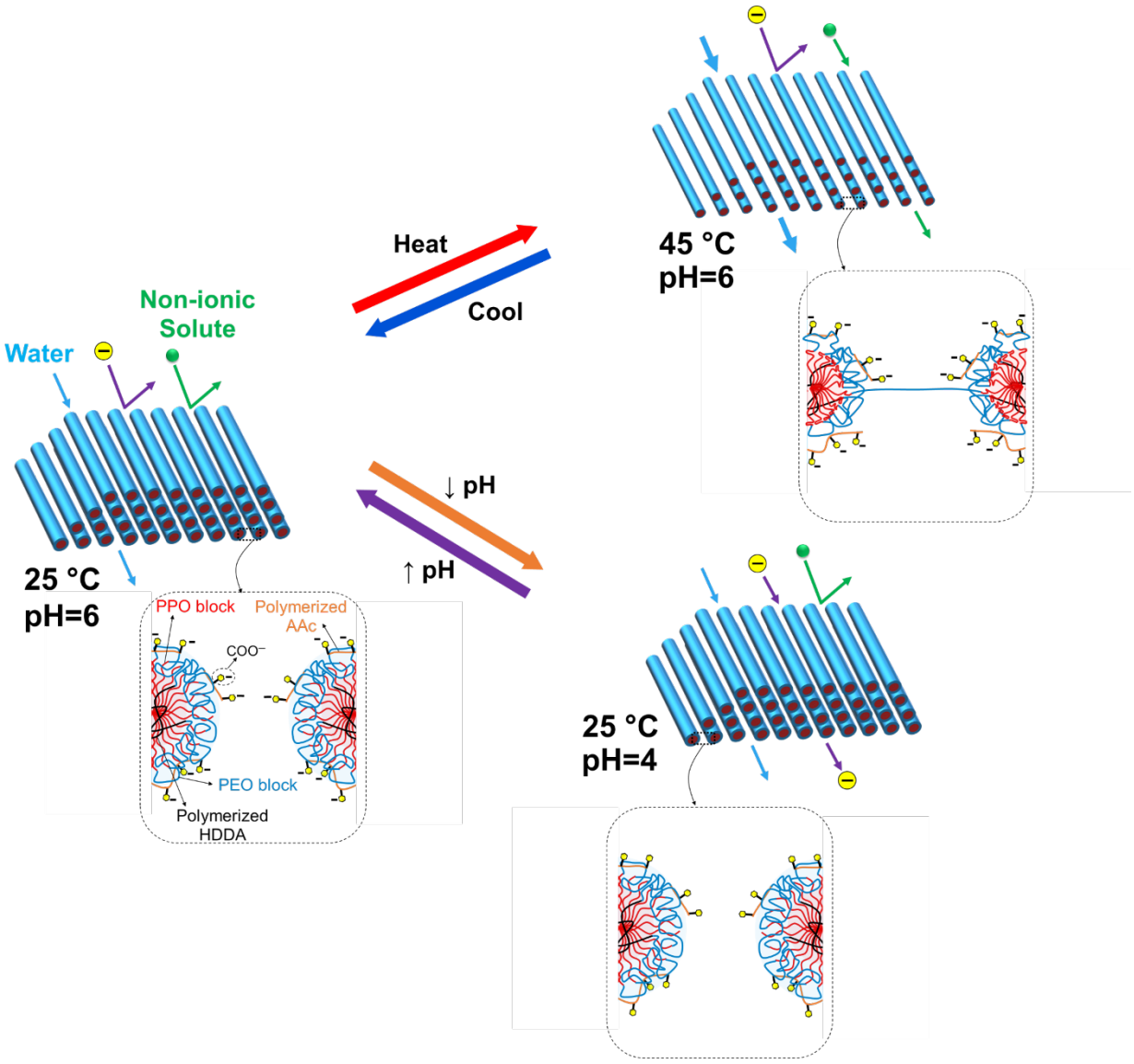

Fig. 9. Schematic illustration of thermo- and pH-responsiveness mechanisms of the polyLLC membrane.

SUPPORTING INFORMATION

Schematic of Pluronic P84 diacrylation reaction and ^{1}HNMR results for P84DA; structural changes of the mesophase under a heating-cooling cycle; rejection performance of commercially available NF270 membranes including: chloride/sulfate selectivity in the presence of magnesium as a cation without adjusting pH, rejection of sulfate salts at different pH, and rejection of OG at different pH; adsorption of BSA, DR80, and PEG 10 kDa on mesophase after exchanging the IL with water.

ACKNOWLEDGEMENTS

YS, SMT, and RF would like to thank the support by the National Science Foundation (NSF) under grant no. 1840871 and 2212894. This work was performed, in part, at the Center for Integrated Nanotechnologies, an Office of Science User Facility operated for the U.S. Department of Energy (DOE) Office of Science. Los Alamos National Laboratory, an affirmative action equal opportunity employer, is managed by Triad National Security, LLC for the U.S. DOE's NNSA, under contract 89233218CNA000001.

CONFLICT OF INTEREST

The authors declare that they have no conflict of interest.

REFERENCES

(1) Wang, K.; Wang, X.; Januszewski, B.; Liu, Y.; Li, D.; Fu, R.; Elimelech, M.; Huang, X. Tailored Design of Nanofiltration Membranes for Water Treatment Based on Synthesis-Property-Performance Relationships. *Chemical Society Reviews*. 2022, pp 672–719. https://doi.org/10.1039/d0cs01599g.

(2) Ahmad, N. N. R.; Ang, W. L.; Teow, Y. H.; Mohammad, A. W.; Hilal, N. Nanofiltration Membrane Processes for Water Recycling, Reuse and Product Recovery within Various Industries: A Review. *J. Water Process Eng.* **2022**, *45*, 102478. https://doi.org/10.1016/j.jwpe.2021.102478.

(3) Roy, Y.; Lienhard, J. H. A Framework to Analyze Sulfate: Versus Chloride Selectivity in Nanofiltration. *Environ. Sci. Water Res. Technol.* **2019**, *5* (3), 585–598. https://doi.org/10.1039/c8ew00847g.

(4) Lu, D.; Yao, Z.; Jiao, L.; Waheed, M.; Sun, Z.; Zhang, L. Separation Mechanism, Selectivity Enhancement Strategies and Advanced Materials for Mono-/Multivalent Ion-Selective Nanofiltration Membrane. *Advanced Membranes*. 2022, p 100032. https://doi.org/10.1016/j.advmem.2022.100032.

(5) Zhang, Y.; Kim, D.; Dong, R.; Feng, X.; Osuji, C. O. Tunable Organic Solvent Nanofiltration in Self-Assembled Membranes at the Sub-1 Nm Scale. *Sci. Adv.* **2022**, *8* (11). https://doi.org/10.1126/sciadv.abm5899.

(6) Cao, Y.; Chen, G.; Wan, Y.; Luo, J. Nanofiltration Membrane for Bio-Separation: Process-Oriented Materials Innovation. *Engineering in Life Sciences*. June 20, 2021, pp 405–416. https://doi.org/10.1002/elsc.202000100.

(7) Dong, X.; Al-Jumaily, A.; Escobar, I. C. Investigation of the Use of a Bio-Derived Solvent for Non-Solvent-Induced Phase Separation (NIPS) Fabrication of Polysulfone Membranes. *Membranes (Basel).* **2018**, *8* (2), 23. https://doi.org/10.3390/membranes8020023.

(8) Mohamat, R. Fabrication of Nanofiltration Membrane Utilising Surfactant Via Non-Solvent

Induced Phase Separation Method. *SPEKTRA J. Kaji. Pendidik. Sains* **2019**, *5* (2), 129. https://doi.org/10.32699/spektra.v5i2.108.

(9) Zhang, L.; Zhang, R.; Ji, M.; Lu, Y.; Zhu, Y.; Jin, J. Polyamide Nanofiltration Membrane with High Mono/Divalent Salt Selectivity via Pre-Diffusion Interfacial Polymerization. *Journal of Membrane Science*. October 2021, p 119478. https://doi.org/10.1016/j.memsci.2021.119478.

(10) Li, X.; Cao, Y.; Yu, H.; Kang, G.; Jie, X.; Liu, Z.; Yuan, Q. A Novel Composite Nanofiltration Membrane Prepared with PHGH and TMC by Interfacial Polymerization. *J. Memb. Sci.* **2014**, *466*, 82–91. https://doi.org/10.1016/j.memsci.2014.04.034.

(11) Yuan, S.; Zhang, G.; Zhu, J.; Mamrol, N.; Liu, S.; Mai, Z.; Van Puyvelde, P.; Van Der Bruggen, B. Hydrogel Assisted Interfacial Polymerization for Advanced Nanofiltration Membranes. *J. Mater. Chem. A* **2020**, *8* (6), 3238–3245. https://doi.org/10.1039/c9ta12984g.

(12) Kahrs, C.; Schwellenbach, J. Membrane Formation via Non-Solvent Induced Phase Separation Using Sustainable Solvents: A Comparative Study. *Polymer (Guildf).* **2020**, *186*, 122071. https://doi.org/10.1016/j.polymer.2019.122071.

(13) Zhang, Y.; Dong, R.; Gabinet, U. R.; Poling-Skutvik, R.; Kim, N. K.; Lee, C.; Imran, O. Q.; Feng, X.; Osuji, C. O. Rapid Fabrication by Lyotropic Self-Assembly of Thin Nanofiltration Membranes with Uniform 1 Nanometer Pores. *ACS Nano* **2021**, *15* (5), 8192–8203. https://doi.org/10.1021/acsnano.1c00722.

(14) Zhang, R.; Zhu, Y.; Zhang, L.; Lu, Y.; Yang, Z.; Zhang, Y.; Jin, J. Polyamide Nanofiltration Membranes from Surfactant-Assembly Regulated Interfacial Polymerization: The Effect of Alkyl Chain. *Macromol. Chem. Phys.* **2021**, *222* (20). https://doi.org/10.1002/macp.202100222.

(15) Hyde, S. T. Identification of Lyotropic Liquid Crystalline Mesophases. In *Handbook of Applied Surface and Colloid Chemistry*; John Wiley & Sons New York, 2001; Vol. 2, pp 299–332.

(16) Saadat, Y.; Imran, O. Q.; Osuji, C. O.; Foudazi, R. Lyotropic Liquid Crystals as Templates for Advanced Materials. *Journal of Materials Chemistry A*. 2021, pp 21607–21658. https://doi.org/10.1039/d1ta02748d.

(17) Feng, X.; Imran, Q.; Zhang, Y.; Sixdenier, L.; Lu, X.; Kaufman, G.; Gabinet, U.; Kawabata, K.; Elimelech, M.; Osuji, C. O. Precise Nanofiltration in a Fouling-Resistant Self-Assembled Membrane with Water-Continuous Transport Pathways. *Sci. Adv.* **2019**, *5* (8). https://doi.org/10.1126/sciadv.aav9308.

(18) Dischinger, S. M.; Rosenblum, J.; Noble, R. D.; Gin, D. L.; Linden, K. G. Application of a Lyotropic Liquid Crystal Nanofiltration Membrane for Hydraulic Fracturing Flowback Water: Selectivity and Implications for Treatment. *J. Memb. Sci.* **2017**, *543*, 319–327. https://doi.org/10.1016/j.memsci.2017.08.028.

(19) McLaughlin, J. R.; Abbott, N. L.; Guymon, C. A. Responsive Superabsorbent Hydrogels via Photopolymerization in Lyotropic Liquid Crystal Templates. *Polymer (Guildf).* **2018**, *142*, 119–126. https://doi.org/10.1016/j.polymer.2018.03.016.

(20) Pindzola, B. A.; Jin, J.; Gin, D. L. Cross-Linked Normal Hexagonal and Bicontinuous Cubic Assemblies via Polymerizable Gemini Amphiphiles. *J. Am. Chem. Soc.* **2003**, *125* (10), 2940–2949.

https://doi.org/10.1021/ja0208106.

(21) Carter, B. M.; Wiesenauer, B. R.; Hatakeyama, E. S.; Barton, J. L.; Noble, R. D.; Gin, D. L. Glycerol-Based Bicontinuous Cubic Lyotropic Liquid Crystal Monomer System for the Fabrication of Thin-Film Membranes with Uniform Nanopores. *Chem. Mater.* **2012**, *24* (21), 4005–4007. https://doi.org/10.1021/cm302027s.

(22) Gin, D. L.; Carter, B. M.; Wiesenauer, B. R.; Hatakeyama, E. S.; Noble, R. D.; Barton, J. L. Method and Membrane for Nanoporous, Bicontinuous Cubic Lyotropic Liquid Crystal Polymer Membranes That Enable Facile Film Processing and Pore Size Control. U.S. Patent Application No. 14/234,362., June 5, 2014.

(23) Zhou, M.; Nemade, P. R.; Lu, X.; Zeng, X.; Hatakeyama, E. S.; Noble, R. D.; Gin, D. L. New Type of Membrane Material for Water Desalination Based on a Cross-Linked Bicontinuous Cubic Lyotropic Liquid Crystal Assembly. *J. Am. Chem. Soc.* **2007**, *129* (31), 9574–9575. https://doi.org/10.1021/ja073067w.

(24) Carter, B. M.; Wiesenauer, B. R.; Noble, R. D.; Gin, D. L. Thin-Film Composite Bicontinuous Cubic Lyotropic Liquid Crystal Polymer Membranes: Effects of Anion-Exchange on Water Filtration Performance. *J. Memb. Sci.* **2014**, *455*, 143–151. https://doi.org/10.1016/j.memsci.2013.12.056.

(25) Choi, J. Y.; Yun, T.; Kwak, S. Y. Two-Step Thermoresponsive Membrane with Tunable Separation Properties and Improved Cleaning Efficiency. *J. Memb. Sci.* **2018**, *554*, 117–124. https://doi.org/10.1016/j.memsci.2018.02.060.

(26) Saadat, Y.; Kim, K.; Foudazi, R. Two-Step Thermoresponsive Ultrafiltration Membranes from Polymerization of Lyotropic Liquid Crystals. *ACS Appl. Polym. Mater.* **2022**, *4* (11), 8156–8165. https://doi.org/10.1021/acsapm.2c01095.

(27) Zhao, X.; Su, Y.; Chen, W.; Peng, J.; Jiang, Z. PH-Responsive and Fouling-Release Properties of PES Ultrafiltration Membranes Modified by Multi-Functional Block-like Copolymers. *J. Memb. Sci.* **2011**, *382* (1–2), 222–230. https://doi.org/10.1016/j.memsci.2011.08.014.

(28) Sinha, M. K.; Purkait, M. K. Preparation and Characterization of Novel Pegylated Hydrophilic PH Responsive Polysulfone Ultrafiltration Membrane. *J. Memb. Sci.* **2014**, *464*, 20–32. https://doi.org/10.1016/j.memsci.2014.03.067.

(29) Fu, J.; Wang, X.; Ma, Z.; Wenming, H.; Li, J.; Wang, Z.; Wang, L. Photocatalytic Ultrafiltration Membranes Based on Visible Light Responsive Photocatalyst: A Review. *Desalin. Water Treat.* **2019**, *168*, 42–55. https://doi.org/10.5004/dwt.2019.24403.

(30) Xiang, T.; Lu, T.; Zhao, W. F.; Zhao, C. S. Ionic Strength- and Thermo-Responsive Polyethersulfone Composite Membranes with Enhanced Antifouling Properties. *New J. Chem.* **2018**, *42* (7), 5323–5333. https://doi.org/10.1039/c8nj00039e.

(31) Sinha, M. K.; Purkait, M. K. Preparation of a Novel Thermo Responsive PSF Membrane, with Cross Linked PVCL-Co-PSF Copolymer for Protein Separation and Easy Cleaning. *RSC Adv.* **2015**, *5* (29), 22609–22619. https://doi.org/10.1039/c4ra13863e.

(32) Saadat, Y.; Tabatabaei, S. M.; Kim, K.; Foudazi, R. Thermoresponsive Antifouling Ultrafiltration Membranes from Mesophase Templating. *J. Memb. Sci.* **2023**, *684*, 121861.

https://doi.org/10.1016/j.memsci.2023.121861.

(33) Zhu, Q.; Liu, Y.; Zuo, P.; Dong, Y.; Yang, Z.; Xu, T. An Isoporous Ion Exchange Membrane for Selective Na+ Transport. *J. Memb. Sci.* **2022**, *659*, 120805. https://doi.org/10.1016/j.memsci.2022.120805.

(34) Li, P.; Johnson, C.; Dyer, S. S.; Osuji, C. O.; Gin, D. L. A PH- and Light-Responsive Nanoporous Lyotropic Gyroid Polymer Network. *Adv. Mater. Interfaces* **2023**, *10* (5), 2201761. https://doi.org/10.1002/admi.202201761.

(35) Himstedt, H. H.; Marshall, K. M.; Wickramasinghe, S. R. PH-Responsive Nanofiltration Membranes by Surface Modification. *J. Memb. Sci.* **2011**, *366* (1–2), 373–381. https://doi.org/10.1016/j.memsci.2010.10.027.

(36) Wu, C.; Zhao, L.; Zhang, Y. PH-Responsive Nanofiltration Membranes Based on Porphyrin Supramolecular Self-Assembly by Layer-by-Layer Technique. *RSC Adv.* **2017**, *7* (75), 47397–47406. https://doi.org/10.1039/c7ra08568k.

(37) Himstedt, H. H.; Du, H.; Marshall, K. M.; Wickramasinghe, S. R.; Qian, X. PH Responsive Nanofiltration Membranes for Sugar Separations. *Ind. Eng. Chem. Res.* **2013**, *52* (26), 9259–9269. https://doi.org/10.1021/ie400982p.

(38) Weng, X. D.; Bao, X. J.; Jiang, H. D.; Chen, L.; Ji, Y. L.; An, Q. F.; Gao, C. J. PH-Responsive Nanofiltration Membranes Containing Carboxybetaine with Tunable Ion Selectivity for Charge-Based Separations. *J. Memb. Sci.* **2016**, *520*, 294–302. https://doi.org/10.1016/j.memsci.2016.08.002.

(39) Setiawan, O.; Huang, Y. H.; Abdi, Z. G.; Hung, W. S.; Chung, T. S. PH-Tunable and PH-Responsive Polybenzimidazole (PBI) Nanofiltration Membranes for Li+/Mg2+ Separation. *J. Memb. Sci.* **2023**, *668*, 121269. https://doi.org/10.1016/j.memsci.2022.121269.

(40) Tan, S.; Saito, K.; Hearn, M. T. Stimuli-Responsive Polymeric Materials for Separation of Biomolecules. *Curr. Opin. Biotechnol.* **2018**, *53*, 209–223. https://doi.org/10.1016/j.copbio.2018.02.011.

(41) Hatakeyama, E. S.; Gabriel, C. J.; Wiesenauer, B. R.; Lohr, J. L.; Zhou, M.; Noble, R. D.; Gin, D. L. Water Filtration Performance of a Lyotropic Liquid Crystal Polymer Membrane with Uniform, Sub-1-Nm Pores. *J. Memb. Sci.* **2011**, *366* (1–2), 62–72. https://doi.org/10.1016/j.memsci.2010.09.028.

(42) López-Barrón, C. R.; Chen, R.; Wagner, N. J.; Beltramo, P. J. Self-Assembly of Pluronic F127 Diacrylate in Ethylammonium Nitrate: Structure, Rheology, and Ionic Conductivity before and after Photo-Cross-Linking. *Macromolecules* **2016**, *49* (14), 5179–5189. https://doi.org/10.1021/acs.macromol.6b00205.

(43) Cellesi, F.; Tirelli, N.; Hubbell, J. A. Materials for Cell Encapsulation via a New Tandem Approach Combining Reverse Thermal Gelation and Covalent Crosslinking. *Macromol. Chem. Phys.* **2002**, *203* (10–11), 1466–1472. https://doi.org/10.1002/1521-3935(200207)203:10/11<1466::AID-MACP1466>3.0.CO;2-P.

(44) Qavi, S.; Lindsay, A. P.; Firestone, M. A.; Foudazi, R. Ultrafiltration Membranes from

Polymerization of Self-Assembled Pluronic Block Copolymer Mesophases. *J. Memb. Sci.* **2019**, *580*, 125–133. https://doi.org/10.1016/j.memsci.2019.02.060.

(45) Kestin, J.; Sokolov, M.; Wakeham, W. A. Viscosity of Liquid Water in the Range Ã¢Ëâ8Ã¢â¬â°ÃÂ°C to 150Ã¢â¬â°ÃÂ°C. *J. Phys. Chem. Ref. Data* **1978**, *7* (3), 941–948. https://doi.org/10.1063/1.555581.

(46) Christensen, D. A. Darcy's Law: Pressure-Driven Transport Through Membranes; Christensen, D. A., Ed.; Springer International Publishing: Cham, 2009; pp 15–26. https://doi.org/10.1007/978-3-031-01636-3_2.

(47) Tu, S. C.; Ravindran, V.; Den, W.; Pirbazari, M. Predictive Membrane Transport Model for Nanofiltration Processes in Water Treatment. *AIChE J.* **2001**, *47* (6), 1346–1362. https://doi.org/10.1002/aic.690470612.

(48) Chang, J. H.; Ohno, M.; Esumi, K.; Meguro, K. Interaction of Iodine with Nonionic Surfactant and Polyethylene Glycol in Aqueous Potassium Iodide Solution. *J. Am. Oil Chem. Soc.* **1988**, *65* (10), 1664–1668. https://doi.org/10.1007/BF02912573.

(49) Davey, C. J.; Low, Z.-X.; Wirawan, R. H.; Patterson, D. A. Molecular Weight Cut-off Determination of Organic Solvent Nanofiltration Membranes Using Poly(Propylene Glycol). *J. Memb. Sci.* **2017**, *526*, 221–228. https://doi.org/10.1016/j.memsci.2016.12.038.

(50) McCormick, D. T.; Stovall, K. D.; Guymon, C. A. Photopolymerization in Pluronic Lyotropic Liquid Crystals: Induced Mesophase Thermal Stability. *Macromolecules* **2003**, *36* (17), 6549–6558. https://doi.org/10.1021/ma030037e.

(51) Alexandridis, P.; Olsson, U.; Lindman, B. A Record Nine Different Phases (Four Cubic, Two Hexagonal, and One Lamellar Lyotropic Liquid Crystalline and Two Micellar Solutions) in a Ternary Isothermal System of an Amphiphilic Block Copolymer and Selective Solvents (Water and Oil). *Langmuir* **1998**, *14* (10), 2627–2638. https://doi.org/10.1021/la971117c.

(52) Qavi, S.; Bandegi, A.; Firestone, M.; Foudazi, R. Polymerization in Soft Nanoconfinement of Lamellar and Reverse Hexagonal Mesophases. *Soft Matter* **2019**, *15* (41), 8238–8250. https://doi.org/10.1039/c9sm01565e.

(53) Alexandridis, P.; Olsson, U.; Lindman, B. Self-Assembly of Amphiphilic Block Copolymers: The (EO)13(PO)30(EO)13–Water–p-Xylene System. *Macromolecules* **1995**, *28* (23), 7700–7710. https://doi.org/10.1021/ma00127a016.

(54) Qavi, S.; Foudazi, R. Rheological Characteristics of Mesophases of Block Copolymer Solutions. *Rheol. Acta* **2019**, *58* (8), 483–498. https://doi.org/10.1007/s00397-019-01162-y.

(55) Alexandridis, P.; Olsson, U.; Lindman, B. Phase Behavior of Amphiphilic Block Copolymers in Water-Oil Mixtures: The Pluronic 25R4-Water-p-Xylene System. *J. Phys. Chem.* **1996**, *100* (1), 280–288. https://doi.org/10.1021/jp951626s.

(56) Kushan, E.; Senses, E. Thermoresponsive and Injectable Composite Hydrogels of Cellulose Nanocrystals and Pluronic F127. *ACS Appl. Bio Mater.* **2021**, *4* (4), 3507–3517. https://doi.org/10.1021/acsabm.1c00046.

(57) Chatterjee, S.; Hui, P. C. leung; Kan, C. wai; Wang, W. Dual-Responsive (PH/Temperature) Pluronic F-127 Hydrogel Drug Delivery System for Textile-Based Transdermal Therapy. *Sci. Rep.* **2019**, *9* (1), 11658. https://doi.org/10.1038/s41598-019-48254-6.

(58) Deliormanlı, A. M.; Türk, M. Flow Behavior and Drug Release Study of Injectable Pluronic F-127 Hydrogels Containing Bioactive Glass and Carbon-Based Nanopowders. *J. Inorg. Organomet. Polym. Mater.* **2020**, *30* (4), 1184–1196. https://doi.org/10.1007/s10904-019-01346-2.

(59) Lee, C. F.; Tseng, H. W.; Bahadur, P.; Chen, L. J. Synergistic Effect of Binary Mixed-Pluronic Systems on Temperature Dependent Self-Assembly Process and Drug Solubility. *Polymers (Basel).* **2018**, *10* (1), 105. https://doi.org/10.3390/POLYM10010105.

(60) Ijaz, Q. A.; Abbas, N.; Arshad, M. S.; Hussain, A.; Shahiq-uz-Zaman; Javaid, Z. Synthesis and Evaluation of PH Dependent Polyethylene Glycol-Co-Acrylic Acid Hydrogels for Controlled Release of Venlafaxine HCl. *J. Drug Deliv. Sci. Technol.* **2018**, *43*, 221–232. https://doi.org/10.1016/j.jddst.2017.10.010.

(61) Chiu, H.-C.; Wu, A.-T.; Lin, Y.-F. Synthesis and Characterization of Acrylic Acid-Containing Dextran Hydrogels. *Polymer (Guildf).* **2001**, *42* (4), 1471–1479. https://doi.org/10.1016/S0032-3861(00)00523-1.

(62) Silberberg-Bouhnik, M.; Ramon, O.; Ladyzhinski, I.; Mizrahi, S.; Cohen, Y. Osmotic Deswelling of Weakly Charged Poly(Acrylic Acid) Solutions and Gels. *J. Polym. Sci. Part B Polym. Phys.* **1995**, *33* (16), 2269–2279. https://doi.org/10.1002/polb.1995.090331612.

(63) Durpekova, S.; Di Martino, A.; Dusankova, M.; Drohsler, P.; Sedlarik, V. Biopolymer Hydrogel Based on Acid Whey and Cellulose Derivatives for Enhancement Water Retention Capacity of Soil and Slow Release of Fertilizers. *Polymers (Basel).* **2021**, *13* (19), 3274. https://doi.org/10.3390/polym13193274.

(64) Chen, Z.; Luo, J.; Hang, X.; Wan, Y. Physicochemical Characterization of Tight Nanofiltration Membranes for Dairy Wastewater Treatment. *J. Memb. Sci.* **2018**, *547*, 51–63. https://doi.org/10.1016/j.memsci.2017.10.037.

(65) Mänttäri, M.; Pekuri, T.; Nyström, M. NF270, a New Membrane Having Promising Characteristics and Being Suitable for Treatment of Dilute Effluents from the Paper Industry. *J. Memb. Sci.* **2004**, *242* (1–2), 107–116. https://doi.org/10.1016/j.memsci.2003.08.032.

(66) Hernández, S.; Porter, C.; Zhang, X.; Wei, Y.; Bhattacharyya, D. Layer-by-Layer Assembled Membranes with Immobilized Porins. *RSC Adv.* **2017**, *7* (88), 56123–56136. https://doi.org/10.1039/c7ra08737c.

(67) Chudoba, R.; Heyda, J.; Dzubiella, J. Temperature-Dependent Implicit-Solvent Model of Polyethylene Glycol in Aqueous Solution. *J. Chem. Theory Comput.* **2017**, *13* (12), 6317–6327. https://doi.org/10.1021/acs.jctc.7b00560.

(68) Özdemir, C.; Güner, A. Solution Thermodynamics of Poly(Ethylene Glycol)Water Systems. *J. Appl. Polym. Sci.* **2006**, *101* (1), 203–216. https://doi.org/10.1002/app.23191.

(69) Dang, H. Q.; Price, W. E.; Nghiem, L. D. The Effects of Feed Solution Temperature on Pore Size and Trace Organic Contaminant Rejection by the Nanofiltration Membrane NF270. *Sep. Purif.*

Technol. **2014**, *125*, 43–51. https://doi.org/10.1016/j.seppur.2013.12.043.

(70) Flecha, F. L. G.; Levi, V. Determination of the Molecular Size of BSA by Fluorescence Anisotropy. *Biochem. Mol. Biol. Educ.* **2003**, *31* (5), 319–322. https://doi.org/10.1002/bmb.2003.494031050261.

(71) Lin, J.; Ye, W.; Baltaru, M. C.; Tang, Y. P.; Bernstein, N. J.; Gao, P.; Balta, S.; Vlad, M.; Volodin, A.; Sotto, A.; Luis, P.; Zydney, A. L.; Van der Bruggen, B. Tight Ultrafiltration Membranes for Enhanced Separation of Dyes and Na2SO4 during Textile Wastewater Treatment. *J. Memb. Sci.* **2016**, *514*, 217–228. https://doi.org/10.1016/j.memsci.2016.04.057.

(72) Khademi, M.; Barz, D. P. J. Structure of the Electrical Double Layer Revisited: Electrode Capacitance in Aqueous Solutions. *Langmuir* **2020**, *36* (16), 4250–4260. https://doi.org/10.1021/acs.langmuir.0c00024.

(73) Rayner-Canham, G.; Overton, T. *Descriptive Inorganic Chemistry*; Macmillan, 2003.

(74) Wiśniewska, M.; Urban, T.; Grządka, E.; Zarko, V. I.; Gun'ko, V. M. Comparison of Adsorption Affinity of Polyacrylic Acid for Surfaces of Mixed Silica-Alumina. *Colloid Polym. Sci.* **2014**, *292* (3), 699–705. https://doi.org/10.1007/s00396-013-3103-x.

(75) Boo, C.; Wang, Y.; Zucker, I.; Choo, Y.; Osuji, C. O.; Elimelech, M. High Performance Nanofiltration Membrane for Effective Removal of Perfluoroalkyl Substances at High Water Recovery. *Environ. Sci. Technol.* **2018**, *52* (13), 7279–7288. https://doi.org/10.1021/acs.est.8b01040.

(76) Werber, J. R.; Osuji, C. O.; Elimelech, M. Materials for Next-Generation Desalination and Water Purification Membranes. *Nature Reviews Materials*. April 5, 2016, p 16018. https://doi.org/10.1038/natrevmats.2016.18.

(77) Rana, D.; Matsuura, T. Surface Modifications for Antifouling Membranes. *Chem. Rev.* **2010**, *110* (4), 2448–2471. https://doi.org/10.1021/cr800208y.

(78) Kelly, S. T.; Zydney, A. L. Mechanisms for BSA Fouling during Microfiltration. *J. Memb. Sci.* **1995**, *107* (1–2), 115–127. https://doi.org/10.1016/0376-7388(95)00108-O.

(79) Mo, H.; Tay, K. G.; Ng, H. Y. Fouling of Reverse Osmosis Membrane by Protein (BSA): Effects of PH, Calcium, Magnesium, Ionic Strength and Temperature. *J. Memb. Sci.* **2008**, *315* (1–2), 28–35. https://doi.org/10.1016/j.memsci.2008.02.002.

(80) Hoffman, J. R.; Phillip, W. A. Dual-Functional Nanofiltration Membranes Exhibit Multifaceted Ion Rejection and Antifouling Performance. *ACS Appl. Mater. Interfaces* **2020**, *12* (17), 19944–19954. https://doi.org/10.1021/acsami.0c03075.